NASA/TM–2014-218151

Analysis and Simulation of the Simplified Aircraft-Based Paired Approach Concept With the ALAS Alerting Algorithm in Conjunction With Echelon and Offset Strategies

Wilfredo Torres-Pomales, Michael M. Madden, Ricky W. Butler, and Raleigh B. Perry
Langley Research Center, Hampton, Virginia

January 2014

NASA STI Program . . . in Profile

Since its founding, NASA has been dedicated to the advancement of aeronautics and space science. The NASA scientific and technical information (STI) program plays a key part in helping NASA maintain this important role.

The NASA STI program operates under the auspices of the Agency Chief Information Officer. It collects, organizes, provides for archiving, and disseminates NASA's STI. The NASA STI program provides access to the NASA Aeronautics and Space Database and its public interface, the NASA Technical Report Server, thus providing one of the largest collections of aeronautical and space science STI in the world. Results are published in both non-NASA channels and by NASA in the NASA STI Report Series, which includes the following report types:

- TECHNICAL PUBLICATION. Reports of completed research or a major significant phase of research that present the results of NASA Programs and include extensive data or theoretical analysis. Includes compilations of significant scientific and technical data and information deemed to be of continuing reference value. NASA counterpart of peer-reviewed formal professional papers, but having less stringent limitations on manuscript length and extent of graphic presentations.

- TECHNICAL MEMORANDUM. Scientific and technical findings that are preliminary or of specialized interest, e.g., quick release reports, working papers, and bibliographies that contain minimal annotation. Does not contain extensive analysis.

- CONTRACTOR REPORT. Scientific and technical findings by NASA-sponsored contractors and grantees.

- CONFERENCE PUBLICATION. Collected papers from scientific and technical conferences, symposia, seminars, or other meetings sponsored or co-sponsored by NASA.

- SPECIAL PUBLICATION. Scientific, technical, or historical information from NASA programs, projects, and missions, often concerned with subjects having substantial public interest.

- TECHNICAL TRANSLATION. English-language translations of foreign scientific and technical material pertinent to NASA's mission.

Specialized services also include organizing and publishing research results, distributing specialized research announcements and feeds, providing information desk and personal search support, and enabling data exchange services.

For more information about the NASA STI program, see the following:

- Access the NASA STI program home page at *http://www.sti.nasa.gov*

- E-mail your question to help@sti.nasa.gov

- Fax your question to the NASA STI Information Desk at 443-757-5803

- Phone the NASA STI Information Desk at 443-757-5802

- Write to:
  STI Information Desk
  NASA Center for AeroSpace Information
  7115 Standard Drive
  Hanover, MD 21076-1320

NASA/TM–2014-218151

Analysis and Simulation of the Simplified Aircraft-Based Paired Approach Concept With the ALAS Alerting Algorithm in Conjunction With Echelon and Offset Strategies

Wilfredo Torres-Pomales, Michael M. Madden, Ricky W. Butler, and Raleigh B. Perry
Langley Research Center, Hampton, Virginia

National Aeronautics and
Space Administration

Langley Research Center
Hampton, Virginia 23681-2199

January 2014

Available from:

NASA Center for AeroSpace Information
7115 Standard Drive
Hanover, MD 21076-1320
443-757-5802

Abstract

This report presents analytical and simulation results of an investigation into proposed operational concepts for closely spaced parallel runways, including the Simplified Aircraft-based Paired Approach (SAPA) with alerting and an escape maneuver, MITRE's echelon spacing and no escape maneuver, and a hybrid concept aimed at lowering the visibility minima. We found that the SAPA procedure can be used at 950 ft separations or higher with next-generation avionics and that 1150 ft separations or higher is feasible with current-rule compliant ADS-B OUT. An additional 50 ft reduction in runway separation for the SAPA procedure is possible if different glideslopes are used. For the echelon concept we determined that current generation aircraft cannot conduct paired approaches on parallel paths using echelon spacing on runways less than 1400 ft apart and next-generation aircraft will not be able to conduct paired approach on runways less than 1050 ft apart. The hybrid concept added alerting and an escape maneuver starting 1 NM from the threshold when flying the echelon concept. This combination was found to be effective, but the probability of a collision can be seriously impacted if the turn component of the escape maneuver has to be disengaged near the ground (e.g. 300 ft or below) due to airport buildings and surrounding terrain. We also found that stabilizing the approach path in the straight-in segment was only possible if the merge point was at least 1.5 to 2 NM from the threshold unless the total system error can be sufficiently constrained on the offset path and final turn.

Table of Contents

Acronyms

3D	Three-Dimensional
ADS-B	Automatic Dependent Surveillance - Broadcast
AGL	Above Ground Level
AILS	Airborne Information for Lateral Spacing
ALAS	Adjacent Landing Alerting System
ALE	ADS-B OUT Latency Error
ALT HLD	Altitude Hold mode
API	Application Programming Interface
APP	Approach mode
ATC	Air Traffic Control
CAS	Calibrated Air Speed
CAT	Instrument Landing System Category
CFH	Collision-Free Height
CMF	Cockpit Motion Facility
CONOPS	Concept of Operations
CSPR	Closely Spaced Parallel Runways
DOT	Department of Transportation
EAS	Equivalent Airspeed
EPU	Estimated Position Uncertainty
FAA	Federal Aviation Administration
FAF	Final Approach Fix
FMC	Flight Management Computer
GPS	Global Positioning System
GS	Groundspeed
HDG	Heading mode
HDG SEL	Heading Select mode
HITL	Human-in-the-Loop
IGE	In-Ground Effect
ILS	Instrument Landing System
IMC	Instrument Meteorological Conditions
IS	Intruder Ship
KEAS	Knots Equivalent Airspeed
LDA	Localizer Type Directional Aid
LOC	Localizer mode
MASPS	Minimum Aviation System Performance Standard
MCP	Mode Control Panel
MSL	Mean Sea-Level
MOPS	Minimum Operational Performance Standard
NACp	Navigation Accuracy Category for Position
NACv	Navigation Accuracy Category for Velocity
NE	Navigation Error
NGE	Near Ground Effect
OGE	Out-of-Ground Effect
OS	Ownship
PRM	Precision Runway Monitor
RNAV	Area Navigation
RNP	Required Navigation Performance
RTCA	Radio Technical Commision for Aeronautics

RWY	Runway
SAP	Stabilized Approach Point
SAPA	Simplified Aircraft-based Paired Approach
SFO	San Francisco International Airport
SPD	Speed mode
tALAS	Test simulation for ALAS
TAS	True Air Speed
TBR	To Be Resolved
TCA	Time of Closest Approach
TCAS	Traffic Alert and Collision Avoidance System
TCH	Threshold Crossing Height
TSE	Total System Error
UTC	Coordinated Universal Time
VERT SPD	Vertical Speed mode
VMC	Visual Meteorological Conditions
WAAS	Wide Area Augmentation System

1. Introduction

In our previous work, we developed an alerting algorithm and Java/C++ software implementations called ALAS [Perry2013]. ALAS (Adjacent Landing Alerting System) is an alerting algorithm designed to detect intrusions on closely spaced parallel runways. It employs a mechanism for detecting imminent collisions with the adjacent traffic aircraft and a mechanism for detecting lateral deviations from the runway centerline in a manner similar to the Precision Runway Monitor system [Shank1994]. The algorithm is highly configurable through a set of user-specifiable parameters. We also developed a fast-time simulation called tAlas, which was able to simulate about 20,000 parallel approaches per minute. The tAlas simulation was used to evaluate the ALAS algorithm in the context of a parallel runway separated by 750 ft. The ALAS algorithm was also validated using the high-fidelity Cockpit Motion Facility (CMF) simulation running on a desktop [Smith2000].

This report documents follow-on work conducted in fiscal year 2013. In this work we (1) analyzed the use of the ALAS algorithm in the context of various runway spacings, (2) explored the potential benefits of using echelon spacing on parallel approaches, (3) investigated the potential benefits (e.g. lower minima) of a hybrid procedure where both echelon spacing is used until reaching a distance of 1 NM from the threshold and then the ALAS algorithm is applied, and (4) developed a new runway conformance algorithm for an offset runway.

2. SAPA Procedure For Various Runway Spacings

In this section we use both fast-time and high-fidelity simulation to investigate the capability of the ALAS alerting algorithm to maintain safety for various runway spacings. The fast-time simulation provides statistically-significant evidence while the high-fidelity simulation is used to confirm the results of the fast-time simulation.

2.1. Fast Time Simulation

In our previous work [Perry2013] we developed a fast time simulation to test the performance of the ALAS algorithm for a runway spacing of 750 ft. A worst-case analysis was performed using this simulation and the CMF high-fidelity simulation. The trajectories generated by the fast-time simulation did not match the CMF trajectories because the kinematic models used in the tAlas simulation were too simple. In this work, we have improved the tAlas simulation [Perry2013] in 7 ways:

1. It can now run as a Monte Carlo simulation in addition to a worst-case simulation.

2. The kinematic turn was improved to include roll-in and roll-out. (This change resulted in an escape maneuver that more closely matches the trajectory generated in the CMF high-fidelity simulation).

3. The vertical acceleration ramps up for escapeVsRampTime seconds.

4. ADS-B latency times were added.

5. ADS-B position errors are modeled.

6. The ground speed profile was improved.

7. The total system error (TSE) decreases linearly as the aircraft approaches the runway (see Figure 2-1). TSE has a value of 25 ft at the runway and 131 ft at 5 NM away. The threshold TSE is a little below the acceptable TSE of 27 ft for touchdown [Kayton1997] and the 5 NM TSE matches the observed 40 m TSE for RNP legs in the terminal area [MITRE2013].

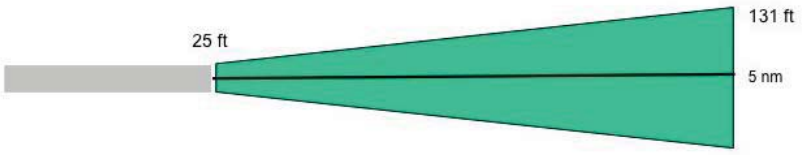

Figure 2-1: Total System Error decreases as the aircraft approaches its runway

We have applied the tAlas simulation to two situations: (1) various parallel runways spacings

using a 3 s ADS-B latency time consistent with the FAA ADS-B Rule [FAA2010 & RTCA2011] and (2) various parallel runways spacings using a 1.5 s ADS-B latency time achievable with state-of-the-art technology that complies with standard DO-260B [RTCA2002, RTCA2009, and RTCA2011].

The revised tAlas can execute about 10,000 parallel approaches per minute, which is roughly half the number of the previous version of the simulation.

2.1.1. ALAS Algorithm Parameters

The ALAS algorithm has remained unchanged since our previous report [Perry2013] except that we have added a capability to perform conformance monitoring for an offset approach (See Appendix A). For the reader's convenience we restate the meaning of the ALAS algorithm parameters in this section.

The ALAS parameters fall into three broad categories: (1) parameters that define the line-based conflict detection region, (2) parameters that control the algorithm, and (3) parameters used by the runway conformance tests.

Line-based Detection Parameter	Meaning	Default Value
ln_front_buffer_red	Length of the red-alert buffer in front of aircraft	10,000 ft
ln_back_buffer_red	Length of red-alert buffer in back of aircraft	800 ft
ln_T_red	Lookahead time for red alert	15 s
ln_front_buffer_yellow	Length of yellow-alert buffer in front of aircraft	10000 ft
ln_back_buffer_yellow	Length of yellow-alert buffer in back of aircraft	1400 ft
ln_T_yellow	Lookahead time for yellow alert	35 s

Internal Parameters	Meaning	Default Value
useAbsDistAwayAlg	True if additional distance test is used	true
initHeight	Altitude difference where algorithm turns on	MAX_VALUE
numPtsTrkRateCalc	Number of data points used in track rate calculation	3
maxPhi	Highest bank angle used in search	40°
phiIncr	Bank angle increment in search	5°
trackRateThreshold	Track rate threshold that triggers the bank-angle sweeep search	1.0°/s
absDistRed	Mininimum horizontal distance that triggers a red alert	486.5 ft
absDistYellow	Mininimum horizontal distance that triggers a yellow alert	545.4 ft

Runway Conformance Parameter	Meaning	Default Value
redRunwayDist	Distance from centerline that triggers a red alert	170 ft
yellowRunwayDist	Distance from centerline that triggers a yellow alert	140 ft

We have changed one ALAS parameter, yellowRunwayDist, from 132 ft to 140 ft. This change was necessary to reduce nuisance yellow alerts in the presence of the newly added ADS-B position errors.

2.1.2. The tALAS Simulator

The test simulation for ALAS (tALAS) is based on kinematic models of the ownship and intruder aircraft trajectories. Figure 2-2 to Figure 2-4 illustrate these models and identify some of the key parameters.

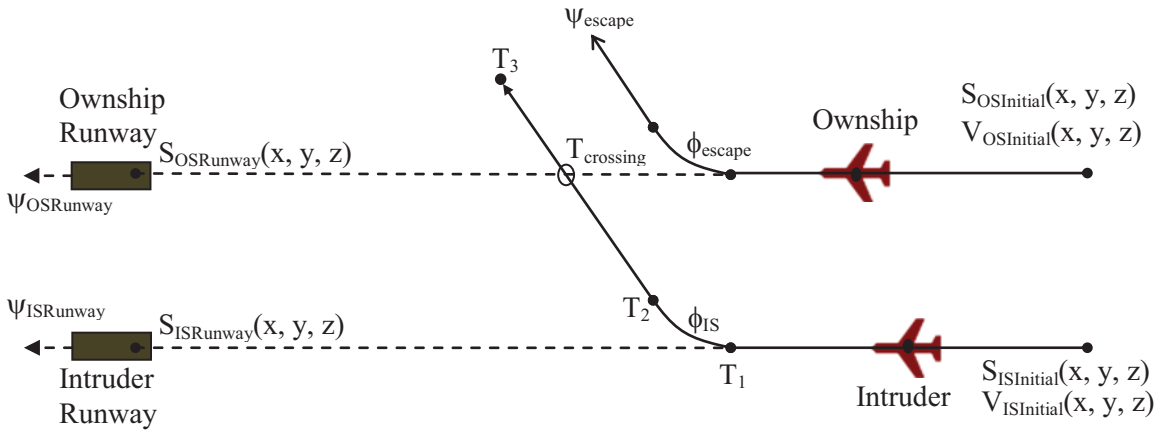

Figure 2-2: Top view of landing trajectory with blunder and escape maneuver

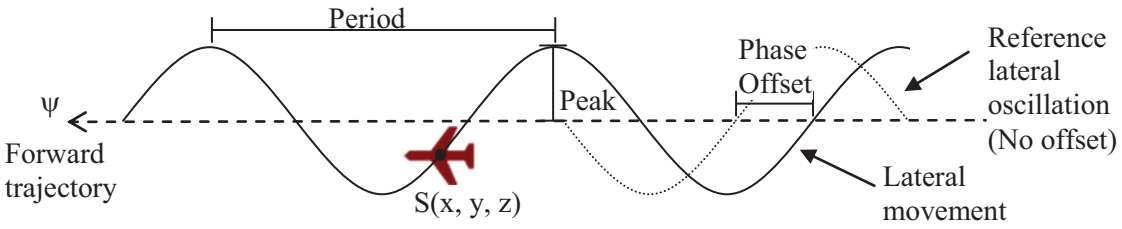

Figure 2-3: Top view of lateral deviation

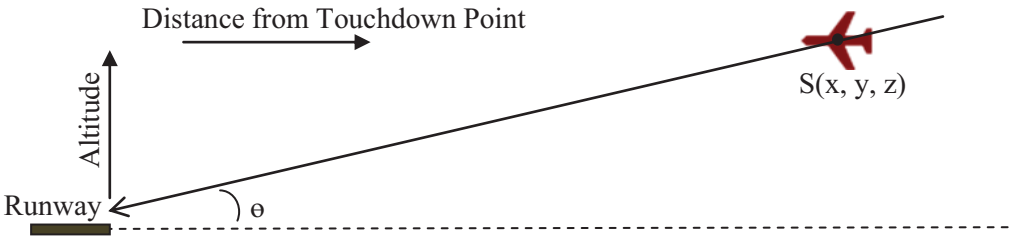

Figure 2-4: Side view of landing trajectory

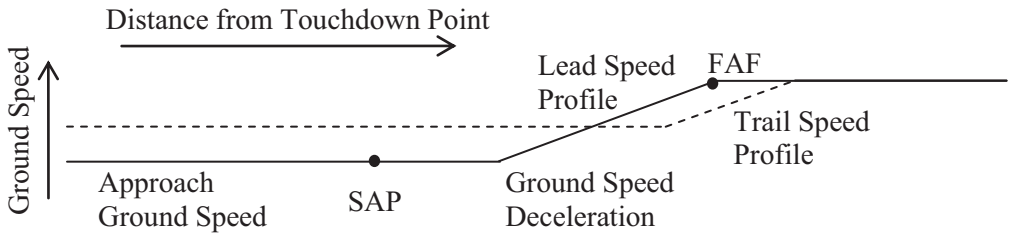

Figure 2-5: Ground speed profiles for landing

The flight trajectory for the ownship is a straight-line descent following the glide path with an optional escape maneuver. The trajectory for the intruder can be either a normal or a blundered landing approach. The trajectories are specified separately and are independently executed until there is a red alert from ALAS, which triggers an escape maneuver by the ownship. The following paragraphs describe the trajectory parameters for the ownship and intruder aircraft.

2.1.2.1. tAlas Trajectories

A trajectory has independent forward and lateral components. The forward trajectory component specifies the desired path of travel. The lateral component simulates the tracking error or wandering that happens due to, for example, wind gusts or control system limit cycles. A simple sinusoidal oscillation model is used for the lateral deviation. As shown in Figure 2-3**,** this lateral oscillation is superposed on the forward trajectory and is specified by three parameters: peak amplitude, time period, and phase offset. The amplitude of the lateral oscillation decays linearly as the aircraft approach the runways to simulate an increase in accuracy and the aircraft actually touching down on their respective runways. The trajectories for the ownship and intruder have independently specified lateral oscillations. Vector addition is used to combine the forward and lateral components for a trajectory's position and velocity.

The ownship landing trajectory is specified relative to the position and heading for landing on the runway. The position of the runway is specified by the touchdown point, denoted $\mathbf{S}_{\mathbf{OSRunway}}$ in Figure 2-2. The runway heading is denoted $\psi_{\mathbf{OSRunway}}$. The initial position $\mathbf{S}_{\mathbf{OSInitial}}$ and velocity $V_{\mathbf{OSInitial}}$ are specified to match the desired descent profile with a specified glideslope angle. An escape is triggered by a red alert from ALAS with a specified pilot delay from the time of the alert to the beginning of the maneuver. An escape maneuver consists of a vertical climb at a constant vertical acceleration and an optional turn away from the intruder. The vertical acceleration model has a ramp-up delay after which the acceleration is sustained until the vertical speed reaches a specified value. If the escape is initiated above the optional designated minimum altitude for an escape turn, the ownship turns to heading $\psi_{\mathbf{escape}}$ with bank angle $\phi_{\mathbf{escape}}$. Otherwise, the escape maneuver does not include a change in heading. A turn has an optional roll time to simulate the time for the bank angle to reach $\phi_{\mathbf{escape}}$. After completing the escape maneuver, the ownship continues in a straight line with the specified heading and climbing.

The intruder trajectory is a straight-line descent with an optional blunder. In Figure 2-2, the runway touchdown point and heading are denoted $\mathbf{S}_{\mathbf{ISRunway}}$ and $\psi_{\mathbf{ISRunway}}$. The initial position $\mathbf{S}_{\mathbf{OSInitial}}$ and velocity $V_{\mathbf{OSInitial}}$ are specified to match the desired descent profile with a specified glideslope angle. A blunder consists of a turn inward toward the ownship with a bank angle $\phi_{\mathbf{IS}}$

turn and a roll time. The turn is executed from time T1 to T2 after which the intruder continues in a straight line. The blunder may also include a leveling out component beginning at time T1 + TLevel with an optional ramp up delay in the vertical acceleration and continuing until a constant altitude is reached.

At the beginning of a landing case, the aircraft are positioned on the glidepath at or beyond the FAF point with the aircraft with lower approach speed ahead of the aircraft with higher approach speed. Both aircraft begin the scenario at approximately the same ground speed (between 175 KT and 185 KT) and decelerate to reach their respective approach speeds at or before the SAP point. The vertical speed is coordinated with the ground speed to ensure that the aircraft remain on the glidepath. Alternatively, the aircraft may be initially positioned just before the SAP point with their respective final approach speeds.

2.1.2.2. tAlas ADS-B Error Model

The tAlas simulation incorporates an ADS-B model with position update delay and error components [Eftekari2008]. The position update delay is a single parameter that covers the end-to-end processing and communication delay. The position error model has only a horizontal bias component and no altitude error component. The horizontal position error has two components, a bias that remains constant for an entire trajectory and a jitter component that is recomputed every simulation step. The horizontal bias is modeled in polar coordinates with radial and angular coordinates (r, θ) given by $r = N(0, \sigma_{HFOM})$ and $\theta = U(0, 2\pi)$, where r follows a Normal distribution with 0 mean and σ_{HFOM} standard deviation, and θ has a uniform distribution around a full circle. The parameter σ_{HFOM} denotes the standard deviation of the GPS horizontal figure of merit (HFOM). The jitter component of the position error is an additional radial error term given by $\delta = \{-0.05\sigma_{HFOM}$ for $p \leq 0.5$, $0.05\sigma_{HFOM}$ for $p > 0.5\}$, where $p = U(0, 1)$. There is no jitter for the angular position error. The reported ADS-B position in Cartesian coordinates is given by $(x_{ADS\text{-}B}, y_{ADS\text{-}B})$ with $x_{ADS\text{-}B} = x + e_x$ and $y_{ADS\text{-}B} = y + e_y$, where (x, y) is the actual horizontal position and (e_x, e_y) is the position error given by $e_x = (r + \delta)\cos(\theta)$ and $e_y = (r + \delta)\sin(\theta)$.

2.1.2.3. tAlas Configuration and Parameters

The tAlas simulation has a wide range of scenario configuration options. The basic parameters that change from one case (or trial) to the next during a run specify the initial positions and speeds of the aircraft and the timing of the blunder. The parameter values for a particular trial can be selected either randomly with specified distributions or deterministically within a discretized value range. Runs with random parameter values are intended to determine the probability distribution of the minimum distance and the probability of violating the collision zone. Runs with deterministic parameter selection are intended to explore a range of possible landing cases and discovering worst-case conditions for safety. Additional simulation parameters which remain constant during a set of trials specify the runway spacing, landing trajectories (including headings and glideslope angles), escape and blunder maneuvers, maximum ground speed difference for final approach, lateral tracking error, ADS-B performance (including position error and latency), and ALAS configuration.

The simulation is instrumented to collect data on false alarms, missed alerts, and the distance of closest approach. tAlas also incorporates a collision zone around the aircraft according to the descriptions given in [FAA2011]. Two collision zone models are available in tAlas: a sphere or a cylinder. For each test trial case, tALAS determines: the time of closest approach and the corresponding distance in 3D space, as well as the horizontal and vertical distances; whether there

was an intrusion into the collision zone; whether the intruder crossed the ownship's centerline and the corresponding time of crossing; the time of the first yellow (i.e., level 1) alert; the time of first red (i.e., level 2) alert; whether a given red alert was not preceded by a yellow alert; the elapsed time from the yellow alert to the red alert; the elapsed time from the red alert to the time the intruder crossed the ownship's centerline; whether there was a red alert without a blunder (i.e., a false alarm); and whether there was a violation without a red alert (i.e., a missed alert). tAlas is also instrumented to compute the probability of violation of the collision zone. For a set of test cases, tALAS can identify the case with the overall minimum approach distance and present a complete analysis for it. tALAS generates the test trajectories as time-indexed state sequences. These sequences are processed by the instrumentation, and they can also be written to output files for post-run visualization and analysis.

2.1.2.4. Blunder Trajectory Parameters

The tAlas simulation generates blunders using three time parameters:

T1 = Start Time of Intrusion (s)
T2 = Duration of Intrusion Turn (s)
T3 = Duration after turn (s)

The horizontal profile of a blunder trajectory is illustrated in Figure 2-6.

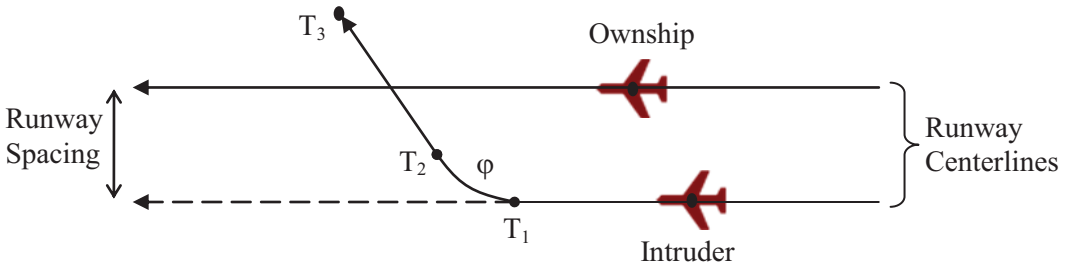

Figure 2-6: Horizontal View for a Blunder Trajectory

tALAS can also create blunders where the intruder's altitude levels out at some point or where it continues to follow its normal vertical profile. If a vertical level-out is specified then the vertical profile is as shown in Figure 2-7.

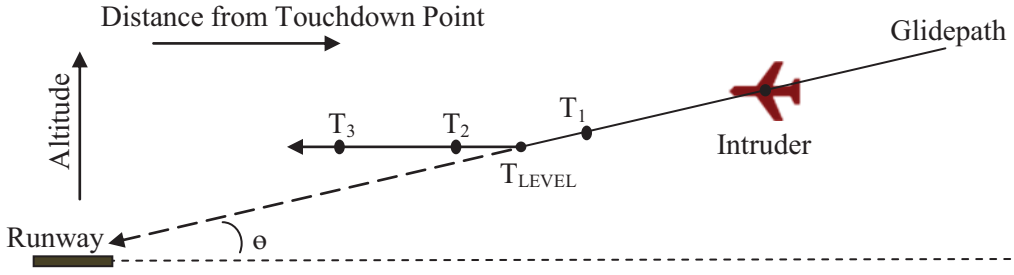

Figure 2-7: Vertical View for a Blunder Trajectory with a Level-out Component

The TLevel parameter, which specifies the time the level-out begins, can appear anytime after T1, the beginning of the intrusion. If a vertical level-out is not specified, then the vertical profile is as shown in Figure 2-8.

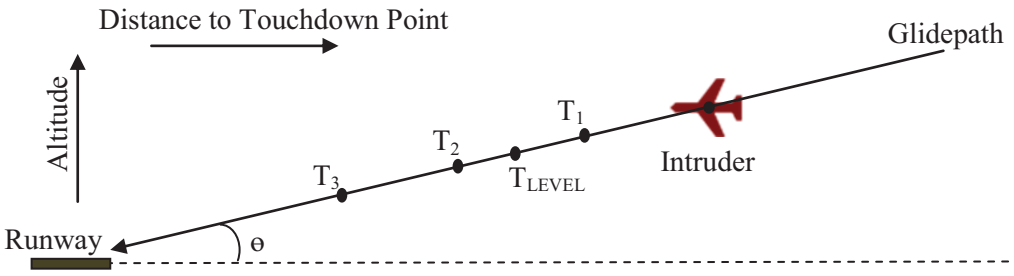

Figure 2-8: Vertical Profile for a Blunder Trajectory without a Level-out Component

The following is stated at the FAA Flight Systems Laboratory, Closely Spaced Parallel Operations (CSPO) website [FAA-CSPO]:

> A blunder occurs when one aircraft on a parallel approach turns toward another aircraft on the adjacent approach. Blunder angle severity and frequency are key parameters in the determination of parallel runway spacing. Blunder data has been collected in its current format since 2008. As of July 31, 2011, there have been over 1.4 million Simultaneous Independent Parallel Instrument Approach (SIPIA) Instrument Landing System (ILS) operations recorded in less than visual conditions. Of those approaches, there have been 60 confirmed blunders which varied in frequency and severity. The verified blunders predominantly occurred at angles between 5° and 35°, with a majority occurring in the 5° to 15° range. Until 2010, the blunder assumption used for fast time simulations was fixed at 30°, a worst case assumption made in the late 1990's necessary to meet the agreed upon level of safety. The assumption was needed since there was no blunder data available at that time. The updated blunder distributions determined from the data collected, along with other updates to model parameters, has contributed to more realistic fast-time simulations and analysis.

In our simulations we have set maxT2 = 14 seconds and uniformly sampled the turn time T2 from [1, maxT2]. We uniformly sample the intruder bank angle between 5 and 30 degrees. This approach results in incidence angles up to 47° with an average incidence angle of 11° which is consistent with the fact that the majority of the historic blunders are within 5° to 15°. We believe that our blunder model is conservative because larger incidence angles are more difficult to defend against. Kinematically, incidence angles larger than 35° can be achieved, especially at larger runway separations.

2.1.2.5. Escape Maneuver Parameters

The parameters in Table 2-1 characterize the escape maneuver that was used.

Table 2-1: Escape Maneuver Parameters

Parameter	Meaning	Nominal Value
escapePilotDelay	Time for pilot to react (s)	0
escapeTrack	Target track delta (°)	45
escapeBankAngle	Bank Angle of Escape Turn (°)	30
escapeRollTime	Time for Rollout to Complete(s)	6
escapeVsGoal	Target vertical speed (fpm)	2000
escapeVsAccel	The vertical acceleration (m/s^2)	2.0
escapeVsRampTime	Time to ramp up to vsAccel (s)	4.0

2.1.2.6. Monte Carlo Simulation: Random Generation of Parameter Values

A probabilistic analysis can be obtained by using random sampling of the parameters over the parameter ranges. In our Monte Carlo experiments, we used the ranges in Table 2-2.

Table 2-2: tALAS Trajectory Parameters (Monte Carlo)

Parameter	Meaning	Min Value	Max Value
T1	Start Time of Intrusion (s)	0	Computed (Description given below)
T2	Duration of Intrusion Turn (s)	1	14
T3	Duration after turn (s)	20	20
bankAngle	Bank Angle of Intrusion (°)	5	30
Peak	Max Trajectory error (ft)	131	131
Period	Period of Trajectory error (s)	60	70
Phase	Phase of Trajectory error (°)	-180	+180
ownshipInitialSx	Distance from runway (NM)	5.0	5.5
intruderInitialSx	Distance from runway (NM)	5.0	5.5
InitialGs	Ground Speed at FAF (KT)	175	185
gsMean	Mean GS at SAP (KT)	130	130
gsSigma	Standard Deviation GS at SAP (KT)	10	10
maxGsDiff	Max GS Differential at SAP (KT)	20	20

The ground speeds of the aircraft decrease from the FAF to the SAP. The simulation starts each aircraft on the glideslope near the FAF. The initial ground speed is uniformly sampled from an interval of 175 KT to 185 KT. The speeds at the SAP are sampled from a normal distribution with a mean of gsMean and a standard deviation of gsSigma. Samples that exceed the minimum or maximum are discarded. Also the ground speeds are sampled such that their difference is less than or equal to maxGsDiff. Once the ground speeds are selected, the time (T1_max) until the intruder reaches an altitude of minAltitudeBlunder is computed. By default minAltitudeBlunder is 0. The blunder time (T1) is then uniformly sampled from the interval [0, T1_max]. After T1, the trial continues an additional extraTimePerTrial seconds, which is typically 90 seconds. We allow blunders to occur when the intruder is close to the ground. However, if the ownship is already on the ground and the intruder's trajectory has not crossed the ownship's centerline and there has been no loss of separation and no alert, this test case is not counted. Removing these trials increases the loss of separation (LoS) probabilities slightly. When the intruder hits the

ground, its trajectory is continued at altitude 0. This allows for a collision after the intruder hits the ground and skids into the ownship.

2.1.3. Results from tAlas Simulations For Various Runway Spacings

In this section we present the tAlas estimates of the probability of a collision given a blunder for various runway spacings. We have chosen a target probability of 1E-5/blunder because historical data suggests that the blunder rate is less than 1E-4/landing. This gives us an overall probability of failure of less than 1E-9/landing. In [Eftekari2011] a table is presented that summarizes the rates of aircraft blunders from recent historical data:

Table 2-3: Summary of No Transgression Zone Violations

Deviation (degrees °)	FY2008	FY2009	Total	Rate Per Approach
< 10	12	8	20	2.55E-05
10 – 19	2	6	8	1.02E-05
20 - 29	0	4	4	5.09E-06
Total	14	18	32	4.08E-05

The blunder arrival rate averaged over both years for all deviations was 4.08E-05. In [Eftekari2011], the authors argue that the first digit is uncertain, so they use a blunder rate of 1E-5 and set a target blunder to collision rate of 1E-4. In this paper, we decided to be more conservative and set the blunder rate at 1E-4/landing. With this blunder rate, a collision rate of no greater than 1E-5/blunder is necessary in order to achieve an overall failure rate of 1E-9/landing.

2.1.3.1. Results for a 400-ft Spherical Protection Zone

In this section the probability of the center of gravity of the intruder aircraft entering a spherical protection zone of radius 400 ft around the ownship is calculated using the tAlas simulation. The probabilities and confidence limits were computed using Wilson's Score Method [Wallis2013] at the 99% confidence level. Each row of Table 2-4 was computed using 10,000,000 simulated landings. Acceptable collision probabilities are indicated in blue font and unacceptable probabilities are indicated in red.

Table 2-4: Monte Carlo Simulation Results for Various Runway Spacing

Runway Spacing (ft)	ADS-B Latency (s)	Num Failures	Probability	Minimum Distance (ft)
750	1.5	65,475	6.53E-03 ± 2.55E-05	93.46
850	1.5	11,169	1.12E-03 ± 1.06E-05	178.74
900	1.5	4,158	4.16E-04 ± 6.44E-06	219.25
950	1.5	1,395	1.40E-04 ± 3.74E-06	258.65
1000	1.5	395	3.99E-05 ± 1.99E-06	301.21
1050	1.5	141	9.84E-06 ± 9.81E-07	316.55
1100	1.5	28	3.24E-06 ± 5.49E-07	331.37
1150	1.5	7	1.14E-06 ± 3.03E-07	350.87

Runway Spacing (ft)	ADS-B Latency (s)	Num Failures	Probability	Minimum Distance (ft)
1050	3.0	4,528	4.53E-04 ± 6.73E-06	158.55
1100	3.0	1,812	1.82E-04 ± 4.26E-06	199.20
1150	3.0	618	6.22E-05 ± 2.49E-06	242.78
1200	3.0	188	1.92E-05 ± 1.38E-06	288.44
1250	3.0	43	4.74E-06 ± 6.72E-07	335.35
1300	3.0	0	4.38E-07 ± 1.48E-07	383.04

Using this protection zone, a runway separation of 1100 ft or more is needed to reach the target probability of collision (i.e. less than 1E-05) for an ADS-B latency of 1.5 s. If the ADS-B latency is 3 s, then a runway separation of 1200 ft is required.

2.1.3.2. Results for the FAA Cylinder Protection Zone (SAPA Procedure)

In the FAA document [FAA2011], a cylinder of radius 265 ft and height 160 ft is recommended for collision studies in the terminal area. It is referred to as the Large Cylinder (or Large Hockey Puck). In this model a collision is assumed to occur when the center of gravity of the blundering aircraft penetrates the cylinder containing the target aircraft. Using this cylindrical protection zone, we obtain more optimistic results. Each row of table was generated using 10,000,000 simulated landings.

Using this protection zone, a runway separation of 950 ft or more is needed to reach the target probability of collision (i.e. less than 1E-05) for an ADS-B latency of 1.5 s. If the ADS-B latency is 3 s, then a runway separation of 1150 ft is required.

Table 2-5: Simulation Results for Various Runway Spacing: Cylinder

Runway Spacing (ft)	ADS-B Latency (s)	Num Los	Probability	Minimum Distance (ft)
750	1.5	5943	5.95E-04 ± 7.71E-06	93.46
850	1.5	679	6.83E-05 ± 2.61E-06	178.74
900	1.5	171	1.75E-05 ± 1.32E-06	219.25
950	1.5	29	3.34E-06 ± 5.58E-07	258.65
1000	1.5	2	6.38E-07 ± 2.05E-07	301.21
1050	1.5	0	4.38E-07 ± 1.48E-07	316.55
1050	3.0	375	3.79E-05 ± 1.94E-06	158.55
1100	3.0	115	1.19E-05 ± 1.08E-06	199.20
1150	3.0	24	2.84E-06 ± 5.12E-07	242.78
1200	3.0	0	4.38E-07 ± 1.48E-07	288.44
1250	3.0	0	4.38E-07 ± 1.48E-07	335.35

These results were obtained using a maximum ground speed difference of 20 KT at the SAP. We included this constraint because the SAPA procedure requires this limitation. Removing this constraint gives us the following collision probabilities.

Table 2-6: Simulation Results for Various Runway Spacing: Cylinder (With No Ground Speed Difference Constraint)

Runway Spacing (ft)	ADS-B Latency (s)	Num Los	Probability	Minimum Distance (ft)
900	1.5	222	2.26E-05 ± 1.50E-06	168.92
950	1.5	52	5.64E-06 ± 7.36E-07	209.21
1000	1.5	10	1.44E-06 ± 3.49E-07	252.98
1050	1.5	0	4.38E-07 ± 1.48E-07	263.79
1050	3.0	397	4.01E-05 ± 2.00E-06	125.60
1100	3.0	145	1.49E-05 ± 1.21E-06	163.67
1150	3.0	30	3.44E-06 ± 5.67E-07	206.35
1200	3.0	6	1.04E-06 ± 2.86E-07	251.74
1250	3.0	0	4.38E-07 ± 1.48E-07	298.61

From Table 2-5 and Table 2-6 we can see that the SAPA ground speed difference constraint reduces the probability of collision slightly. This maximum ground speed difference was primarily imposed to meet the wake vortex requirements, but it provides a minor benefit here as well. Note that either way, a runway separation of 950 ft or more is needed to reach the target probability of collision (i.e. less than 1E-05) for an ADS-B latency of 1.5 s and a runway separation of 1150 ft is required if the ADS-B latency is 3 s.

2.1.3.3. Results for the FAA Cylinder Protection Zone and Different Glideslopes

In this section we present the results of simulations where the intruder's glideslope is at 2.85° and the ownship's glideslope at 3°. The glideslopes at San Francisco International Airport (KSFO), one of the candidate airports for paired approach, were changed in August 2013 to these differentiated angles. Differentiated glideslopes bring potential advantages to the procedure. When the trail is placed on the higher glideslope, its vertical separation from the lead increases with distance from the runway threshold. Therefore, the trail aircraft has a larger vertical separation in those segments of the approach where the total system error (TSE) for each aircraft is also large. Large TSE increases the probable loss of lateral separation between the two aircraft that can occur during normal operation. This decreases the distance that a blundering aircraft or its wake must travel to cross the path of the trail aircraft. However, since neither the wake nor blundering aircraft are assumed to ascend, additional vertical separation between the aircraft increases the possibility that ownship can maintain a safe vertical distance from the wake or blundering aircraft even if it the lateral separation drops below the protection zone radius. A cylindrical protection zone of radius 265 ft and height 160 ft was used. Each row of table was generated using 10,000,000 landings.

Table 2-7: Monte Carlo Simulation Results for Various Runway Spacing with Differing Glideslopes

Runway Spacing (ft)	ADS-B Latency (s)	Num Los	Probability	Minimum Distance (ft)
750	1.5	4316	4.32E-04 ± 6.57E-06	133.91
850	1.5	299	3.03E-05 ± 1.74E-06	206.88
900	1.5	38	4.24E-06 ± 6.34E-07	242.28
950	1.5	3	7.38E-07 ± 2.28E-07	281.18
1000	1.5	0	4.38E-07 ± 1.48E-07	323.15
1000	3.0	526	5.30E-05 ± 2.30E-06	149.79
1050	3.0	129	1.33E-05 ± 1.15E-06	183.14
1100	3.0	22	2.64E-06 ± 4.92E-07	222.62
1150	3.0	2	6.38E-07 ± 2.05E-07	263.71
1200	3.0	0	4.38E-07 ± 1.48E-07	288.44

Comparing this table with Table 2-5 shows that the differing glideslopes provide about 50 ft less runway separation.

2.1.4. Note Concerning Disabling Alert for Trailing Aircraft

The runway performance monitor triggers an ALAS alert for the nearest traffic aircraft even if that aircraft is trailing the ownship by a large distance. The question naturally arises whether there is a longitudinal distance at which the trailing aircraft can be safely ignored. We explored this idea in the tAlas simulation. Our first run was to disable the alert if the longitudinal distance between the aircraft was greater than 750 ft. This led to a surprising result illustrated in Figure 2-9.

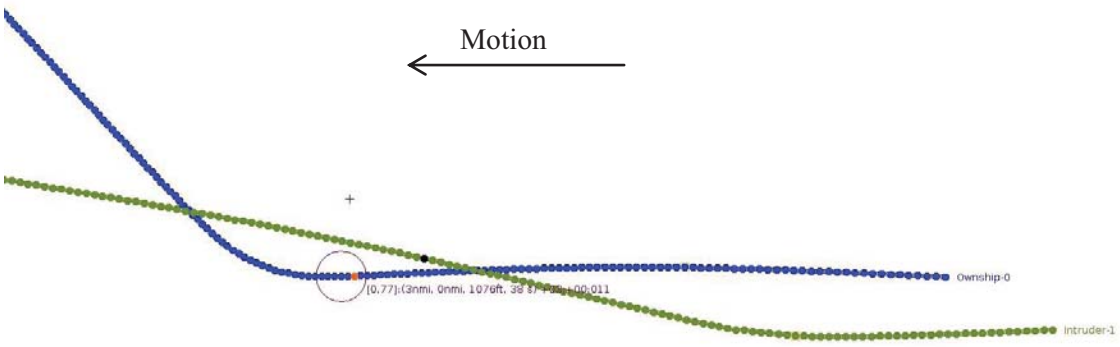

Figure 2-9: Pathological scenario as a result of disabling alerting for trailing aircraft

In this scenario, the intruder has the faster ground speed and is initially more than 750 ft behind the ownship. After the intruder has crossed the path of the ownship, the intruder closes the gap between the two aircraft to a longitudinal distance less than 750 ft. At this point, the

ALAS alert is no longer suppressed (see orange dot). The escape maneuver follows shortly thereafter and a violation of the protection zone occurs. Clearly, if the ownship had not executed the escape maneuver, no LoS would have occurred. Now, there are several tests that could be performed to prevent this from occurring, but first we search for a minimal distance where this is not a problem.

Table 2-8 shows the simulation results for a runway separation of 950 ft, 1.5 s latency and for various longitudinal cutoff distances. Each row was calculated from 10,000,000 simulated landings. Again, acceptable collision probabilities are indicated in blue font and unacceptable probabilities are indicated in red.

Table 2-8: Simulation Results for 950 ft Runway with Various Rear Longitudinal Cutoff Distances

Longitudinal Cutoff Distance (ft)	Probability (large cylinder)	Minimum Distance (ft)
750	1.92E-02 ± 4.34E-05	2.36
1500	1.96E-03 ± 1.40E-05	2.77
2000	3.23E-04 ± 5.68E-06	7.02
2500	2.44E-05 ± 4.71E-06	37.60
3000	3.34E-06 ± 5.58E-07	258.65
3500	3.34E-06 ± 5.58E-07	258.65

From these results we see that an aircraft must be at least trailing 3000 ft or more longitudinally before it can be safely ignored. If it is desirable to disable the ALAS alert for aircraft that are trailing behind, then some additional checks should be added to the ALAS conformance algorithm to insure that it does not engage after the intruder has passed the centerline of the ownship.

2.2. High-fidelity Simulation Results

The 2012 SAPA study [Perry2013] concluded that the SAPA procedure, which allows the trail aircraft to pass the lead aircraft, could not execute safely at a runway separation of 750 feet [Perry2013]. This follow-on study uses the high-fidelity, transport-class aircraft simulation in Langley's Cockpit Motion Facility (CMF) to determine whether safe passing is feasible at a larger runway spacing of 1050 ft for next generation aircraft and whether aircraft adhering to the FAA rule on ADS-B [FAA2010] can safely pass at 1400 ft.

The simulation setup is as described in the 2012 SAPA study [Perry2013] with some small adjustments. In the 2012 SAPA study, the CMF simulation was configured to perform a simultaneous parallel approach to runways 28L and 28R at San Francisco International Airport (KSFO). The lead aircraft was placed assigned to 28L and the trail aircraft was assigned to 28R. The high-fidelity transport model used in the CMF simulation only has the capability to automate instrument landing system (ILS) approaches. Therefore, each aircraft maintains its lateral and vertical path using the localizer and glideslope signals respectively. To provide 1050 ft and 1400 ft runway spacing, the location of KSFO RWY28R and its ILS were shifted the necessary distance in the navigation database. To model current generation aircraft complying with the FAA ADS-B Rule, the latency parameters for ADS-B and ALAS were modified as follows:

- Ownship State
  - Total Latency (Measurement to ALAS input): 1000 ms
  - Compensated Latency: 600 ms
- Traffic State
  - ADS-B OUT
    - Total Latency (Measurement to Transmission): 2000 ms
    - Compensated Latency: 1400 ms
  - ADS-B IN
    - Total Latency (Reception to ALAS): 1000 ms
    - Compensated Latency: 600 ms

The FAA rule-compliant ADS-B has an end-to-end latency of 3 seconds. ADS-B latency parameters for the next generation aircraft is unchanged from the 2012 study and the end-to-end latency is 1.5 seconds.

The method for selecting the initial condition for each run was also modified. In the prior high-fidelity simulation study, the initial position of the trail aircraft was placed at the center of the front and rear gates. In this simulation study, the trail aircraft was positioned to ensure a collision indication in the absence of an escape maneuver. In other words, the initial position of the trail aircraft ensures that separation between lead and trail aircraft is less than 100 feet when the lead aircraft blunders onto the trail's path. Thus, this simulation study can determine whether the collision can be avoided using ALAS and the escape maneuver. However, this simulation study does not examine scenarios where the blunder does not lead to a collision in the absence of an escape maneuver. Therefore, this study cannot assess whether there are circumstances under which the escape maneuver contributes to a collision that would not otherwise occur. As with the 2012 simulation study, this simulation study examined both ideal state inputs to ALAS and inputs with modeled avionics errors and latencies. Furthermore, trials included execution of the blunder and escape maneuver using the stock flight control computer (normal turn) and using an outer-loop control algorithm to superpose a wheel command (augmented turn). All blunders were conducted as a 30° heading change, either while continuing to descend or while leveling off. A blunder in the constant speed segment at 10 NM from the threshold and a blunder after the SAP at 2.5 NM from the threshold were both analyzed.

Table 2-9 through Table 2-12 show the results for 1050 ft runway separation using next-generation avionics with an end-to-end ADS-B latency of 1.5 seconds. Table 2-13 through Table 2-16 show the results for 1400 ft runway separation using current-rule compliant ADS-B with an end-to-end latency of 3 seconds. To identify collisions, a 400-foot collision sphere around the aircraft was used. Within the 96 runs conducted for 1050 ft separation, there are 10 collision indications (in red font). All ten indications occur using normal autopilot turns against blunders where the lead stops its descent. Only one occurs with ideal inputs; the others occur with modeled avionics errors and latencies. These collisions, however, are avoided under more aggressive maneuvering (augmented turn). There are also five false alerts. False alerts are indicated where the alert time is negative. (The latest version of ALAS used to generate the fast-time results in this paper does not produce false alarms when rerun against these CMF trajectories. The ALAS algorithm was adjusted as a consequence of these runs.) Within the 96 runs conducted for 1400 ft separation, there are eight collision indications. Again, these indications occur during normal autopilot turns when the blundering aircraft stops its descent. Furthermore, all occur with modeled avionics errors and latencies. No collision indications occur under more aggressive maneuvering (augmented turn). In addition, no false positive alerts occurred.

These results suggest that it may be possible to perform the SAPA procedure safely at 1050 ft separation with next-generation avionics and at 1400 ft separation with current-rule compliance ADS-B OUT if the automated escape maneuver is programmed to turn more aggressively than under normal autopilot operation.

Table 2-9: 1050 ft Runway Separation - 30° Blunder While Descending During Constant Speed Segment, 1.5 s total latency

	Ideal Input to ALAS					
	Normal Turn			Augmented Turn		
Approach Speeds of Fast/Slow (KT)	Time to Alert (s)	3D Distance at Alert (ft)	Closest 3D Distance (ft)	Time to Alert (s)	3D Distance at Alert (ft)	Closest 3D Distance (ft)
122 / 114	2.12	1038	617	1.62	1034	753
130 / 122	1.70	1046	734	1.08	1038	880
138 / 130	1.92	1061	741	1.32	1047	866
145 / 138	2.00	1063	740	1.36	1051	838
153 / 145	1.86	1087	759	1.60	1069	791
160 / 153	2.74	1116	693	1.94	1093	824

	Modeled Avionics Input to ALAS					
	Normal Turn			Augmented Turn		
Approach Speeds of Fast/Slow (KT)	Time to Alert (s)	3D Distance at Alert (ft)	Closest 3D Distance (ft)	Time to Alert (s)	3D Distance at Alert (ft)	Closest 3D Distance (ft)
122 / 114	3.12	1027	524	3.12	1009	525
130 / 122	3.20	1036	585	2.58	1025	690
138 / 130	3.42	1051	591	2.82	1031	668
145 / 138	3.50	1052	584	2.86	1034	585
153 / 145	2.86	1084	630	3.10	1050	563
160 / 153	3.74	1109	604	2.94	1083	641

Table 2-10: 1050 ft Runway Separation - 30° Blunder While Level During Constant Speed Segment, 1.5 s total latency

	Ideal Input to ALAS					
	Normal Turn			Augmented Turn		
Approach Speeds of Fast/Slow (KT)	Time to Alert (s)	3D Distance at Alert (ft)	Closest 3D Distance (ft)	Time to Alert (s)	3D Distance at Alert (ft)	Closest 3D Distance (ft)
122 / 114	2.24	1044	377	1.24	1040	770
130 / 122	1.96	1061	509	1.02	1047	819
138 / 130	1.58	1062	543	1.24	1045	803
145 / 138	1.56	1064	523	1.28	1057	717
153 / 145	1.66	1083	555	0.94	1082	776
160 / 153	2.60	1103	473	1.54	1089	752

	Modeled Avionics Input to ALAS					
	Normal Turn			Augmented Turn		
Approach Speeds of Fast/Slow (KT)	Time to Alert (s)	3D Distance at Alert (ft)	Closest 3D Distance (ft)	Time to Alert (s)	3D Distance at Alert (ft)	Closest 3D Distance (ft)
122 / 114	3.24	1035	246	2.74	1019	539
130 / 122	2.96	1053	329	3.02	1019	512
138 / 130	3.58	1048	252	2.74	1027	573
145 / 138	3.56	1048	235	2.78	1036	453
153 / 145	3.16	1075	324	2.44	1069	495
160 / 153	4.10	1096	232	2.54	1081	560

Table 2-11: 1050 ft Runway Separation - 30° Blunder While Descending During Final Approach Segment, 1.5 s total latency

	Ideal Input to ALAS					
	Normal Turn			Augmented Turn		
Approach Speeds of Fast/Slow (KT)	Time to Alert (s)	3D Distance at Alert (ft)	Closest 3D Distance (ft)	Time to Alert (s)	3D Distance at Alert (ft)	Closest 3D Distance (ft)
122 / 114	1.44	1567	1201	1.56	1181	904
130 / 122	1.70	1760	1390	1.48	1230	899
138 / 130	1.54	1765	1390	1.10	1138	895
145 / 138	1.86	1111	728	1.52	1201	860
153 / 145	1.90	1154	642	1.12	1192	833
160 / 153	1.64	1592	1157	1.44	1147	785

	Modeled Avionics Input to ALAS					
	Normal Turn			Augmented Turn		
Approach Speeds of Fast/Slow (KT)	Time to Alert (s)	3D Distance at Alert (ft)	Closest 3D Distance (ft)	Time to Alert (s)	3D Distance at Alert (ft)	Closest 3D Distance (ft)
122 / 114	2.94	1550	1041	2.56	1167	763
130 / 122	3.20	1735	1212	1.98	1223	802
138 / 130	3.04	1743	1214	2.60	1109	744
145 / 138	-9.64	1143	1143	3.02	1166	639
153 / 145	-16.10	1261	1253	-13.88	1266	1262
160 / 153	3.14	1561	1014	2.94	1104	577

Table 2-12: 1050 ft Runway Separation - 30° Blunder While Level During Final Approach Segment, 1.5 s total latency

	Ideal Input to ALAS					
	Normal Turn			Augmented Turn		
Approach Speeds of Fast/Slow (KT)	Time to Alert (s)	3D Distance at Alert (ft)	Closest 3D Distance (ft)	Time to Alert (s)	3D Distance at Alert (ft)	Closest 3D Distance (ft)
122 / 114	1.74	1199	720	1.24	1197	941
130 / 122	1.80	1205	703	1.40	1229	810
138 / 130	1.42	1134	602	1.32	1149	837
145 / 138	1.88	1187	586	1.02	1209	894
153 / 145	1.98	1165	501	1.16	1198	804
160 / 153	1.74	1116	463	1.00	1165	773

	Modeled Avionics Input to ALAS					
	Normal Turn			Augmented Turn		
Approach Speeds of Fast/Slow (KT)	Time to Alert (s)	3D Distance at Alert (ft)	Closest 3D Distance (ft)	Time to Alert (s)	3D Distance at Alert (ft)	Closest 3D Distance (ft)
122 / 114	2.74	1187	600	2.74	1177	739
130 / 122	2.30	1197	631	2.90	1196	576
138 / 130	3.42	1090	387	2.82	1111	672
145 / 138	3.88	1148	342	2.52	1182	674
153 / 145	-15.02	1264	1256	-12.84	1263	1260
160 / 153	3.24	1080	255	2.50	1127	552

Table 2-13: 1400 ft Runway Separation - 30° Blunder While Descending During Constant Speed Segment, 3 s total latency

	Ideal Input to ALAS					
	Normal Turn			Augmented Turn		
Approach Speeds of Fast/Slow (KT)	Time to Alert (s)	3D Distance at Alert (ft)	Closest 3D Distance (ft)	Time to Alert (s)	3D Distance at Alert (ft)	Closest 3D Distance (ft)
122 / 114	2.02	1377	869	1.46	1399	1123
130 / 122	1.82	1398	992	1.28	1390	1195
138 / 130	2.08	1410	1001	1.50	1397	1183
145 / 138	1.70	1414	1043	1.18	1406	1198
153 / 145	1.96	1435	1033	1.36	1425	1169
160 / 153	2.36	1467	1014	1.76	1453	1196

	Modeled Avionics Input to ALAS					
	Normal Turn			Augmented Turn		
Approach Speeds of Fast/Slow (KT)	Time to Alert (s)	3D Distance at Alert (ft)	Closest 3D Distance (ft)	Time to Alert (s)	3D Distance at Alert (ft)	Closest 3D Distance (ft)
122 / 114	6.02	1290	445	5.46	1271	585
130 / 122	5.82	1333	556	5.28	1283	649
138 / 130	6.58	1324	493	5.00	1307	701
145 / 138	6.20	1341	556	5.18	1298	588
153 / 145	5.96	1376	632	5.36	1315	564
160 / 153	6.36	1401	576	5.76	1334	554

Table 2-14: 1400 ft Runway Separation - 30° Blunder While Level During Constant Speed Segment, 3 s total latency

	Ideal Input to ALAS					
	Normal Turn			Augmented Turn		
Approach Speeds of Fast/Slow (KT)	Time to Alert (s)	3D Distance at Alert (ft)	Closest 3D Distance (ft)	Time to Alert (s)	3D Distance at Alert (ft)	Closest 3D Distance (ft)
122 / 114	2.14	1410	724	1.08	1404	1143
130 / 122	1.88	1424	831	1.36	1405	1134
138 / 130	2.00	1426	833	1.02	1403	1184
145 / 138	1.58	1435	877	1.12	1421	1098
153 / 145	1.70	1457	921	1.24	1440	1082
160 / 153	2.64	1470	850	1.34	1449	1143

	Modeled Avionics Input to ALAS					
	Normal Turn			Augmented Turn		
Approach Speeds of Fast/Slow (KT)	Time to Alert (s)	3D Distance at Alert (ft)	Closest 3D Distance (ft)	Time to Alert (s)	3D Distance at Alert (ft)	Closest 3D Distance (ft)
122 / 114	6.14	1324	130	5.58	1264	502
130 / 122	4.88	1380	349	5.36	1280	561
138 / 130	6.00	1357	254	5.02	1299	648
145 / 138	6.08	1357	203	5.12	1296	463
153 / 145	5.20	1410	364	5.24	1310	449
160 / 153	6.64	1404	242	5.34	1337	489

Table 2-15: 1400 ft Runway Separation - 30° Blunder While Descending During Final Approach Segment, 3 s total latency

	Ideal Input to ALAS					
	Normal Turn			Augmented Turn		
Approach Speeds of Fast/Slow (KT)	Time to Alert (s)	3D Distance at Alert (ft)	Closest 3D Distance (ft)	Time to Alert (s)	3D Distance at Alert (ft)	Closest 3D Distance (ft)
122 / 114	1.82	1573	1124	1.12	1558	1337
130 / 122	1.44	1606	1190	1.36	1602	1296
138 / 130	1.62	1530	1090	1.16	1509	1250
145 / 138	1.82	1566	1046	1.36	1578	1258
153 / 145	1.88	1535	960	1.48	1552	1151
160 / 153	1.64	1489	959	1.34	1519	1155

	Modeled Avionics Input to ALAS					
	Normal Turn			Augmented Turn		
Approach Speeds of Fast/Slow (KT)	Time to Alert (s)	3D Distance at Alert (ft)	Closest 3D Distance (ft)	Time to Alert (s)	3D Distance at Alert (ft)	Closest 3D Distance (ft)
122 / 114	5.82	1479	764	5.12	1443	865
130 / 122	5.94	1493	786	5.36	1456	803
138 / 130	6.12	1398	669	5.16	1356	865
145 / 138	5.82	1457	649	5.36	1419	731
153 / 145	0.88	1549	1024	5.48	1381	591
160 / 153	5.64	1365	524	4.84	1374	680

Table 2-16: 1400 ft Runway Separation - 30° Blunder While Level During Final Approach Segment, 3 s total latency

	Ideal Input to ALAS					
	Normal Turn			Augmented Turn		
Approach Speeds of Fast/Slow (KT)	Time to Alert (s)	3D Distance at Alert (ft)	Closest 3D Distance (ft)	Time to Alert (s)	3D Distance at Alert (ft)	Closest 3D Distance (ft)
122 / 114	1.48	1580	1112	1.20	1562	1313
130 / 122	1.78	1590	1082	1.40	1611	1213
138 / 130	1.50	1512	960	0.92	1532	1251
145 / 138	1.78	1566	959	1.40	1584	1222
153 / 145	2.00	1549	863	1.22	1587	1180
160 / 153	1.66	1490	826	1.00	1546	1149

	Modeled Avionics Input to ALAS					
	Normal Turn			Augmented Turn		
Approach Speeds of Fast/Slow (KT)	Time to Alert (s)	3D Distance at Alert (ft)	Closest 3D Distance (ft)	Time to Alert (s)	3D Distance at Alert (ft)	Closest 3D Distance (ft)
122 / 114	4.98	1513	743	4.70	1469	892
130 / 122	3.78	1552	861	5.40	1454	661
138 / 130	5.50	1400	522	5.42	1340	795
145 / 138	3.78	1527	692	5.40	1415	689
153 / 145	6.00	1431	380	5.22	1426	626
160 / 153	5.16	1388	348	5.00	1370	630

2.3. Observations

The fast-time and high-fidelity simulations provide evidence that it will be safe to use the SAPA procedure at 1050 ft separations with next-generation avionics and at 1400 ft separations with current-rule compliance ADS-B OUT with an aggressive escape maneuver. The fast time simulations suggest that the SAPA procedure may be used down to 1150 ft separations with current-rule avionics and down to 950 ft separations with future avionics, though this has not yet been validated in the CMF high-fidelity simulation. It seems likely that the use of different glideslopes will reduce the allowed separations by another 50 ft. These results depend upon an automatic, immediate initiation of the escape maneuver. We have modeled the roll time of the turn maneuver and the ramp up of the vertical acceleration in the escape maneuver, but we have not included any delay due to a pilot. We have also assumed that this maneuver can be performed for all possible blunders.

3. Evaluation of Echelon Spacing for Straight-In Procedures

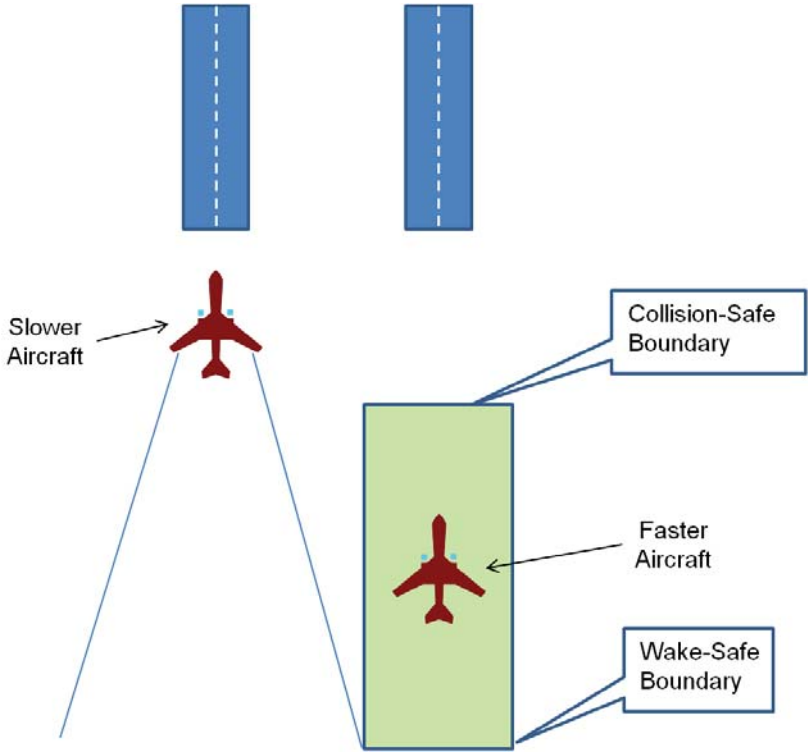

Figure 3-1: Paired Approach with Echelon Spacing

After initial results of the tAlas simulation indicated that the safe runway separation for the SAPA procedure was 1100 ft (see Section 2.1.3.1), NASA was encouraged to investigate the benefits of using echelon spacing. Echelon spacing requires the trail aircraft to maintain a collision-safe distance from the lead aircraft. This section uses statistical analysis to determine the runway separations under which echelon spacing is feasible. Statistical analysis was used in lieu of a Monte-Carlo simulation for two reasons. First, neither the tAlas nor CMF simulations contain a wake transport model useful in determining the wake-safe boundary. Both simulations place the aircraft within pre-established wake-safe boundaries. In the 2012 SAPA Study [Perry 2012], these fast-time simulations used wake-safe boundaries determined from a previous Monte-Carlo study performed by Johnson, et. al. [Johnson 2010]. However, Johnson's results could not be reused for analyzing the Echelon approach due to a difference in wake transport model (see section 3.4.1) and in operating assumptions including total system error, tolerable crosswind, and acceptable probability of a wake encounter. Second, though a new Monte-Carlo simulation could have been developed to determine new wake-safe boundaries, such a simulation would be subject to the same limitations as previous simulations. Namely, the number of runs that are required to characterize, with confidence, wake-safe boundaries with a rarity of 1 encounter in 1 billion flights necessitate long run times. The long run-times hamper iterative redesign of the procedure to converge on a feasible solution. An analytical model can estimate, very rapidly, the wake-safe boundary for a given probability of a wake encounter.

Figure 3-1 depicts the relative geometry of the aircraft in the paired-approach with echelon spacing. The trail aircraft must maintain longitudinal distance from the lead aircraft in a range defined to avoid two hazards, collision and wake. To avoid collision, the trail aircraft must

maintain a sufficient distance from the lead such that the lead will not collide with the trail if the lead blunders towards the trail's path. To avoid wake, the trail aircraft must be close enough to the lead that the wake of the lead aircraft passes behind the trail in the presence of adverse crosswind. The trail must maintain its separation in this range from the loss of altitude separation until the lead aircraft crosses the threshold (TBR[1]). In the constant speed segments, the two aircraft are flying the same speed and the trail can maintain a constant spacing behind the lead. However, after the final approach fix (FAF), both aircraft will slow to their final approach speed. By design, the final approach speed of the trail aircraft is greater than that of the lead aircraft. Therefore, longitudinal separation between the lead and trail will decrease throughout final approach. The trail aircraft must accommodate this compression of longitudinal separation before reaching the FAF to ensure that it will not drop below the collision-safe distance before reaching the threshold. This compression distance grows larger as the approach speed of the lead decreases and as the difference in approach speed between the two vehicles increases.

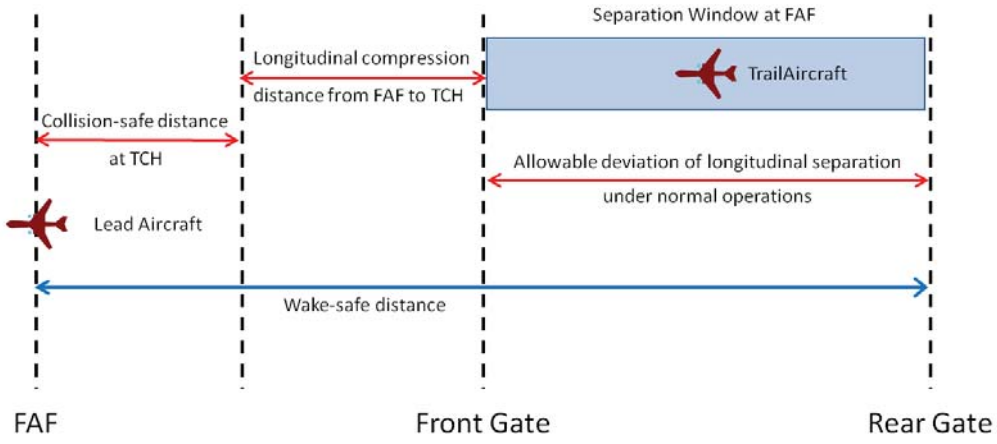

Figure 3-2: Components of Required Longitudinal Separation at the FAF

To determine the feasibility of the procedure for a given pair of aircraft, we must define the collision-safe distance, the longitudinal compression distance, and the wake-safe distance. Figure 3-2 depicts how the collision-safe distance, the longitudinal compression distance, and the wake-safe distance define the required separation between the lead and trail aircraft at the FAF. The collision-safe distance and longitudinal compression distance define the front-gate. The wake-safe distance defines the rear-gate. However, the procedure becomes infeasible for a given pair of aircraft if the distance between the front and rear gate is not long enough to accommodate the deviation in longitudinal separation that can normally occur. Otherwise, the procedure may suffer an ineffectual rate of breakouts. In fact, Section 3.4.3 uses the desired breakout rate to define the normal deviation in longitudinal separation. Some of the variables that determine these distances are subject to variation. These variables include the total system error (TSE) of each aircraft (including its components of flight technical error [FTE] and navigation error [NE]), the error in the ADS-B reported position of the lead aircraft, and the variation in the actual airspeeds of the lead and trail aircraft. Therefore, given a distribution function for these variables (usually assumed to be normal), one can statistically analyze the feasibility of the procedure for a desired

[1] The angle at which the lead aircraft can safely intercept the path of the trail diminishes near the ground. More aggressive maneuvers will lead to ground contact. For this reason, it may be possible to lift longitudinal spacing requirements earlier in the procedure.

probability of successful completion.

3.1. The Collision-Safe Distance

Eftekari, et al. [Eftekari2011] performed an assessment of collision-free separation for parallel approaches at closely spaced parallel runways. Eftekari defined collision-free as a collision probability of 10^{-9} or less divided between a blunder probability of 10^{-5} and a probability of collision after blunder of 10^{-4}. If a blunder can occur at any point in the procedure, this study concluded that the trail aircraft must maintain a longitudinal separation of 750 feet or more within the FAF when the runway spacing is 700 feet. If blunders occur only outside the FAF, Eftekari determined that the longitudinal separation must be 1500 ft or more up to the FAF.

Though Section 4.1 presents NASA's analysis of the collision-safe separation to support the parallel segment of the offset approach to low minima (which also apply to parallel approaches), that work was not completed in time to incorporate into the analysis in this section. Therefore, the analysis in this section establishes a 750 ft minimum separation within the FAF and a 1500 ft minimum separation outside the FAF.

3.2. Longitudinal Compression Distance

Prior to the FAF, the trail aircraft uses speed management to actively control its longitudinal separation with the lead. The trail aircraft stops active management of longitudinal separation when it reaches its final approach speed (by maintaining separation as the lead aircraft's decelerates) or when it reaches the FAF (if it has not detected deceleration by the lead). The trail aircraft will then decelerate to its final approach speed and, since the procedure places the aircraft with the faster approach speed in the trail position, the longitudinal separation will decrease for the remainder of the procedure. However, the trail aircraft continues to monitor the longitudinal separation and will breakout if it drops below the collision-free separation. Therefore, to limit nuisance breakouts, the trail aircraft must position itself to accommodate the longitudinal compression before the aircraft begins to decelerate.

If the aircraft accurately fly their planned approach speed to the threshold, then the longitudinal compression is characterized by the approach speeds of the two vehicles, the rate of deceleration, the minimum separation that must be maintained, the height to which minimum separation must be maintained, winds, and atmospheric density. Winds and atmospheric density come into play because the approach speed is an equivalent airspeed, not a true ground speed. This analysis does not include winds. Nevertheless, headwinds tend to increase the compression distance as it will lead to a decrease in the true ground speed of the lead aircraft and, therefore, increases the time that the trail spends encroaching on the lead. Likewise, tailwinds would tend to decrease the compression distance.

On the other hand, accounting for density with altitude is desirable. At KSFO, assuming a 1976 standard atmosphere, the equivalent airspeed at the FAF is about 3% lower than the true ground speed. From the FAF to touchdown, the elapsed time to threshold is about 3 seconds shorter when one converts EAS to TAS than if one assumes that EAS = TAS. The challenge, however, in computing compression distance by converting EAS to TAS is that the conversion value changes with altitude as density changes with altitude.

Before incorporating the EAS to TAS conversion, let us first determine the kinematic

equations for the approach procedures assuming TAS = EAS. As we will see later, we can formulate the EAS to TAS conversion in a way that allows us to use these same relations. The flight of the lead aircraft is examined first and is shown in Figure 3-3. The lead aircraft's speed schedule can be broken into three segments: a constant speed segment, a deceleration segment, and a final approach segment. The constant speed segment captures the region from where the lead aircraft captures the glideslope until the final approach fix. In this region, the aircraft flies a constant EAS assigned by air traffic control. When the lead aircraft reaches the FAF, it begins the deceleration segment. In this segment, the aircraft decelerates to its planned final approach speed. The deceleration is modeled as a constant that completes the deceleration by the stabilized approach point (SAP) at 1000 ft AGL. After the SAP, the aircraft is in the final approach segment and flies its planned final approach speed to the threshold. The aircraft is expected to initiate a flare maneuver within the neighborhood of the threshold; however, the trail aircraft is no longer required to maintain separation at that point.

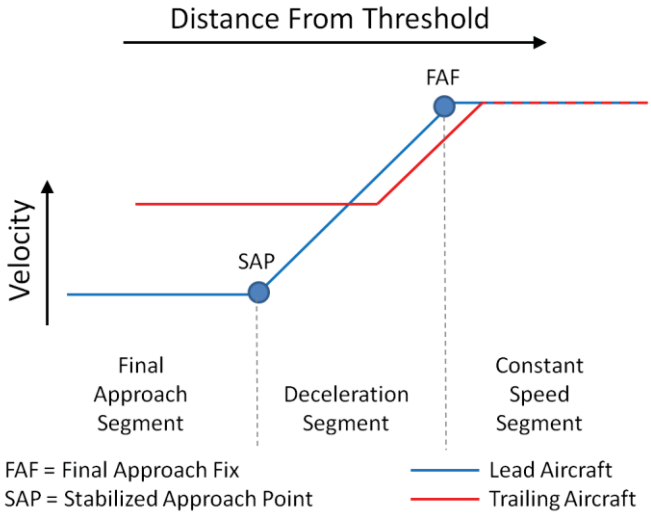

Figure 3-3: Speed Profiles of Lead and Trail Aircraft

To compute the compression distance at the FAF, first calculate the time it takes the lead aircraft to travel from the FAF to the threshold crossing height (TCH). The time from FAF to TCH is divided into two computations: time from FAF to SAP and time from SAP to TCH. The time from FAF to SAP assumes a constant deceleration from the constant segment speed (V_c) to the final approach speed (V_f). Thus, the average speed from FAF to SAP is ½ [V_c + V_f]. Given that the FAF and SAP are defined by height above the runway, the distance between these points is a function of their heights and the glideslope angle. The time is given by:

$$t_{FAF \to SAP} = \frac{D(z,\gamma)}{\bar{V}} = \frac{(z_{FAF} - z_{SAP})}{\sin\gamma} \frac{2}{(V_c + V_f)} \frac{KT}{fps} = \frac{18113}{(V_c + V_f)} \qquad (3\text{-}1)$$

where,

z_{FAF} is the height of the final approach fix in feet, normally 1800 ft

z_{SAP} is the height of the stabilized approach point in feet, normally 1000 ft

γ is the glideslope angle, normal 3°
V_c is the constant segment speed in knots, nominally 180 KT
V_f is the final approach speed in knots
t is the flight time in seconds

Similarly, the time from SAP to TCH is given by:

$$t_{SAP \to TCH} = \frac{D(z,\gamma)}{V} = \frac{(z_{SAP} - z_{TCH})}{V_f \sin\gamma}\frac{KT}{fps} = \frac{10754}{V_f} \quad (3\text{-}2)$$

where, z_{TCH} is the TCH in feet, nominally 50 feet but at KSFO it is 57 ft for the lead aircraft's runway RWY28L and 55 ft for the trail aircraft's runway RWY28R. The total flight time from FAF to TCH for the lead aircraft is therefore,

$$t_{lead} = \frac{18113}{(V_c + V_f)} + \frac{10675}{V_f} \quad (3\text{-}3)$$

For example, if V_c is 180 KT and V_f is 120 KT, then the t_{lead} is 149.3 seconds.

Next, given a starting height at the collision-free distance from the threshold (z_{CFH}), calculate where the trail aircraft would have been t_{lead} seconds in the past. The conditions on the time and rate of deceleration for the trail aircraft complicate this computation. The trail aircraft decelerates at the same rate as the lead aircraft when and if it detects the deceleration of the lead aircraft prior to the trail aircraft reaching the FAF; otherwise, the trail aircraft decelerates independently. One key parameter governing this condition is t_{delay}, the time delay in the response of the trail aircraft to changes in the true state of the lead aircraft. For this study, t_{delay} is assumed to be 5.0 seconds for current generation aircraft and 3.5 seconds for next generation aircraft. Table 3-1 provides a breakdown of the estimated t_{delay}.

Table 3-1: Estimate of Response Delay in Dependent Operations

	Current Generation	Next Generation
ADS-B OUT Latency (from navigation measurement)	2.0 s	0.7 s
ADS-B IN Latency	0.5 s	0.5 s
ALAS Latency	0.5 s	0.3 s
Pilot Reaction Time	2.0 s	2.0 s
Total	5.0 s	3.5 s

Let $t_{I\text{-}Trail}$ be the independent flight time of the trail aircraft from the FAF to z_{CFH}. The trail aircraft will decelerate independently if (t_{lead} - $t_{I\text{-}Trail}$) < t_{delay}. Thus, we first compute $t_{I\text{-}Trail}$. The equations are identical to those for t_{lead} but z_{CFH} is substituted for z_{TCH}.

$$z_{CFH} = z_{TCH} + d_{collision}(tan\,\gamma) = 55\,ft + 750\,ft(tan\,3°) = 94.3\,ft \quad (3\text{-}4)$$

$$t_{SAP \to CFH} = \frac{D(z,\gamma)}{V} = \frac{(z_{SAP} - z_{CFH})}{V_f \sin\gamma}\frac{KT}{fps} = \frac{10253}{V_f} \quad (3\text{-}5)$$

$$t_{I-trail} = t_{FAF \to SAP} + t_{SAP \to CFH} = \frac{18113}{(V_c + V_f)} + \frac{10253}{V_f} \quad (3\text{-}6)$$

If the value of $t_{I\text{-}trail}$ reveals that the trail aircraft will perform an independent deceleration, then the position of the x-axis runway coordinate of the trail aircraft when the lead is at the FAF is:

$$X_{I-trail} = X_{FAF} - \cos\gamma \left(V_c \, (t_{lead} - t_{I-trail}) \frac{fps}{KT} \right) \quad (3\text{-}7)$$

where X_{FAF} is the x-axis runway coordinate of the FAF, nominally -33,392 ft or -5.5 NM; at RWY28R, it is -33297 ft. The above equation is valid as long as $t_{I\text{-}trail} \leq t_{lead}$ which should be true as long as the final approach speed for the trail aircraft is greater than that of the lead aircraft. However, the actual speeds of each aircraft can deviate from their planned speeds. If the trail and lead aircraft have the same planned final approach speed, then the actual speed of the trail aircraft can be lower than planned and, therefore, lower than the actual speed of the lead aircraft. Nevertheless, this situation does not need to be accounted for because as stated in section 3.1, the trail must also maintain a collision-free separation at the FAF of 1500 ft. In fact, given that (t_{lead} - $t_{I\text{-}trail}$) $\leq t_{delay}$, the maximum longitudinal separation at the FAF for independent deceleration of the trail aircraft is $V_c \, t_{delay}$. For next-generation aircraft, a $V_c > 254$ KT would be required to exceed the minimum separation of 1500 ft. That speed is well outside expected variation about the CONOPS designed value of 180 KT [MITRE2013]; therefore, an aircraft pair that could get close enough to allow independent deceleration of the trail, must instead be separated by 1500 ft at the FAF and will perform a dependent deceleration. For current generation aircraft, a $V_c > 178$ KT is required to exceed the minimum separation of 1500 ft. This is within the expected variation about design value of 180 KT; therefore, it remains possible for current generation aircraft to be positioned for an independent deceleration.

If the trail aircraft will perform a dependent deceleration with the lead, the trail aircraft's total flight time, $t_{D\text{-}trail}$, can be broken into three components: t_{delay} - the delay in dependent operation defined in the previous paragraph, t_{decel} - the time to decelerate to the final approach speed, and t_{final} - the time flying at the final approach speed. t_{decel} is computed using the deceleration of the lead aircraft and the final approach speed of the trail aircraft:

$$a_{lead} = \left(\frac{\Delta V}{t_{FAF \to SAP}} \right)_{lead} = (V_f - V_c) \frac{(V_c + V_f)}{2} \frac{\sin\gamma}{(z_{FAF} - z_{SAP})} \frac{fps}{KT} = \frac{(V_f^2 - V_c^2)}{18113} \quad (3\text{-}8)$$

$$t_{decel} = \frac{\Delta V_{trail}}{a_{lead}} = 18113 \frac{(V_f - V_c)_{trail}}{(V_f^2 - V_c^2)_{lead}} \quad (3\text{-}9)$$

Note that the equation for a_{lead} produces an acceleration in units of kt/s so that the equation for t_{decel} produces a time in units of seconds. Now, t_{final} becomes the remaining time, t_{lead} - t_{delay} - t_{decel}. With these times, the x-axis runway coordinate of the trail aircraft performing a dependent deceleration can be computed:

$$X_{D-trail} = -\left(d_{collision} + \cos\gamma \left(V_f \, t_{final} + \tfrac{1}{2}(V_c + V_f) \, t_{decel} + V_c \, t_{delay} \right) \frac{fps}{KT} \right) \quad (3\text{-}10)$$

The compression distance can now be computed for an aircraft pair:

$$d_{compression} = \min_{750}\left(X_{FAF} - d_{collision} - \begin{cases} X_{I-trail}\ if\ (t_{lead} - \mathrm{t_{I-trail}}) \le \mathrm{t_{delay}} \\ X_{D-trail}\ if\ (t_{lead} - \mathrm{t_{I-trail}}) > \mathrm{t_{delay}} \end{cases}\right) \quad (3\text{-}11)$$

The minimum value of $d_{compression}$ is 750 ft since the minimum collision-free separation at the FAF is 1500 ft which is 750 ft greater than $d_{collision}$, the collision-free separation at the threshold. Using the above equations, if the lead aircraft final approach speed is 120 KT and the trail aircraft final approach speed is 130 KT, then the following values would result for the current generation fleet:

t_{lead} = 149.3 seconds
$t_{I\text{-}trail}$ = 137.3 seconds, (t_{lead} - $t_{I\text{-}trail}$) = 12.0 seconds > t_{delay} so compute $X_{D\text{-}trail}$
t_{decel} = 50.3 seconds
$X_{D\text{-}trail}$ = -36014 ft
$d_{compression}$ = 1967 ft

Next, incorporate the EAS to TAS conversion:

$$V_{TAS} = V_{EAS}\sqrt{\frac{\rho}{\rho_0}} = V_{EAS}\sqrt{\frac{P_0\ T}{P\ T_0}} \quad (3\text{-}12)$$

where ρ, P, and T are the atmospheric density, pressure, and temperature respectively and the subscript zero indicates the sea-level value. The second formulation allows the insertion of functions for temperature and pressure from the US Standard 1976 atmosphere model for altitudes below 36,152 ft [NOAA1976]:

$$H = \frac{h\ R_e}{h + R_e} \quad (3\text{-}13)$$

$$T = T_0\left(1 + \frac{H\ L}{T_0}\right) \quad (3\text{-}14)$$

$$P = P_0\left(1 + \frac{H\ L}{T_0}\right)^{-g/(L\ R)} \quad (3\text{-}15)$$

where,

g = the standard acceleration due to free fall, 32.17404 ft/s^2
h = the geometric altitude, feet
L = the lapse rate, -3.56616x10^{-3} °R/ft
P_0 = sea-level pressure, 2116.22 psf
R = the gas constant for air, 1716.55915670803 ft^2/(s^2 °R)
R_e = the radius of the Earth, 20855531.5 ft
T_0 = sea-level temperature, 518.67 °R
H = the geopotential altitude, feet

With these equations, the conversion from EAS to TAS becomes:

$$V_{TAS} = V_{EAS}\sqrt{\left(1 + \frac{h\ L\ R_e}{(h + R_e)T_0}\right)^{1+g/(L\ R)}} = V_{EAS}\sqrt{\left(1 - \frac{143.394\ h}{h + 20855531.5}\right)^{-4.25589}} \quad (3\text{-}16)$$

Equation 3-16 computes TAS as a function of geometric altitude. To determine the distance traveled over a given time, we recognize that TAS is dr/dt where r is the distance along the glideslope. Since the glideslope angle is constant, we can reformulate dr/dt in terms of geometric altitude using the relation h = r sin(γ).

$$V_{TAS} = \frac{dr}{dt} = \left(\csc\gamma \frac{KT}{fps}\right)\frac{dh}{dt} = V_{EAS}\sqrt{\left(1 - \frac{143.394\,h}{h + 20855531.5}\right)^{-4.25589}} \tag{3-17}$$

$$\int dt = t = \left(\frac{\csc\gamma}{V_{EAS}}\frac{KT}{fps}\right)\int \sqrt{\left(1 - \frac{143.394\,h}{h + 20855531.5}\right)^{4.25589}}\, dh \tag{3-18}$$

(Note the change of sign for the exponent in Equation 3-18.) The integral for dh does not have a closed form solution. However, a closed form approximation can be constructed by converting the integrand to a Taylor series and integrating the first two terms:

$$\begin{aligned} t &= \left(\frac{\csc\gamma}{V_{EAS}}\frac{KT}{fps}\right)\int \left(1 - 1.46309\times10^{-5}\,h + 5.74347\times10^{-11}\,h^2 + O(h^3)\right)dh \\ &= \frac{\csc\gamma\ \left(h - 7.31543\times10^{-6}\,h^2\ +\ 1.91449\times10^{-11}\,h^3\right)}{V_{EAS}}\frac{KT}{fps} = \frac{D_{EAS}(h)}{V_{EAS}}\frac{KT}{fps} \end{aligned} \tag{3-19}$$

Note that removing the second and third order terms reduces the equation to the assumption that TAS = EAS. Thus, the second and third order terms represent the effect of accounting for EAS→TAS conversion with altitude on the time to reach sea-level. For example, when starting at an altitude of 1000 ft, the equation indicates that the EAS→TAS conversion is equivalent to reducing the distance traveled by 139 ft. The third order term produces a distance of less than 1 foot below h = 3738 ft. It could be ignored for KSFO given that the geometric altitude of the trail aircraft is expected to be below 2200 ft when the lead aircraft is at the FAF. But the term is kept for future use at other airports whose runways are at an elevation of 1500 ft MSL or greater.

As indicated by the final formulation of Equation 3-19, this equation defines an equivalent airspeed distance term (D_{EAS}) that is a function of geometric altitude. We can substitute D_{EAS} for the z/sin(γ) terms in equations 3-1 through 3-9. For example, the time to travel from SAP to TCH (Equation 3-2), becomes:

$$t_{SAP\to TCH} = \frac{D(h,\gamma)}{V} = \frac{\left(D_{EAS}(h_{SAP}) - D_{EAS}(h_{TCH})\right)}{V_f}\frac{KT}{fps} \tag{3-20}$$

This substitution also works for the deceleration segment when deceleration is assumed to be a constant deceleration of the equivalent airspeed because the deceleration term can then be evaluated in the time integral:

$$V_{TAS} = \left(V_{EAS}^0 + a_{EAS}\,t\right)\sqrt{\left(1 - \frac{143.394\,h}{h + 20855531.5}\right)^{-4.25589}} = \left(\csc\gamma \frac{KT}{fps}\right)\frac{dh}{dt} \tag{3-21}$$

$$\int \left(V_{EAS}^{0} + a_{EAS}\, t\right) \frac{fps}{KT} dt = \csc\gamma \int \sqrt{\left(1 - \frac{143.394\, h}{h + 20855531.5}\right)^{4.25589}}\, dh \tag{3-22}$$

$$\left(V_{EAS}^{0} t + \frac{1}{2} a_{EAS}\, t^2\right) \frac{fps}{KT} = D_{EAS}(h) \tag{3-23}$$

Equation 3-23 is identical to the kinematic equation for constant acceleration for true airspeed with the distance term replaced with D_{EAS}. Finally, equations 3-1 through 3-9, modified to use D_{EAS}, are applied to KSFO. KSFO runways RWY28L and RWY28R are 13 ft above sea-level so the conversion of height above runway (z) to geometric altitude(h) is h = z + 13. Furthermore, RWY28L has a TCH of 57 ft and RWY28R has a TCH of 55 ft. The lead aircraft is placed on RWY 28L. The final equations are:

$$\begin{aligned} t_{lead} &= \left(\frac{\left(\mathrm{D_{EAS}}(1013) - \mathrm{D_{EAS}}(70)\right)}{V_f} + \frac{2\left(\mathrm{D_{EAS}}(1813) - \mathrm{D_{EAS}}(1013)\right)}{V_f + V_c}\right)\frac{KT}{fps} \\ &= \frac{10591}{V_f} + \frac{17741}{V_f + V_c} \end{aligned} \tag{3-24}$$

$$\begin{aligned} t_{I-trail} &= \frac{\left(\mathrm{D_{EAS}}(1013) - \mathrm{D_{EAS}}(68 + \mathrm{d_{collision}} \tan 3°)\right)}{V_f}\frac{KT}{fps} + \frac{17741}{V_f + V_c} \\ &= \frac{10170}{V_f} + \frac{17741}{V_f + V_c} \end{aligned} \tag{3-25}$$

$$a_{lead} = \left(\frac{\Delta V}{t_{FAF \to SAP}}\right)_{lead} = \left(V_f - V_c\right)\frac{V_f + V_c}{17741} = \frac{\left(V_f^2 - V_c^2\right)}{17741} \tag{3-26}$$

$$t_{decel} = \frac{\Delta V_{trail}}{a_{lead}} = 17741\frac{\left(V_f - V_c\right)_{trail}}{\left(V_f^2 - V_c^2\right)_{lead}} \tag{3-27}$$

To compute the X coordinate of the trail aircraft when the lead aircraft is at the FAF, first compute the position as a D_{EAS} distance:

$$D_{I-trail} = D_{EAS}(h_{FAF}) + V_c(t_{lead} - t_{I-trail})\frac{fps}{KT} \tag{3-28}$$

$$\begin{aligned} D_{D-trail} &= \mathrm{D_{EAS}}(68 + 750 \tan 3°) + \left(V_f\, t_{final} + \tfrac{1}{2}\left(V_c + V_f\right) t_{decel} + V_c\, t_{delay}\right)\frac{fps}{KT} \\ &= 2049 + \left(V_f\, t_{final} + \tfrac{1}{2}\left(V_c + V_f\right) t_{decel} + V_c\, t_{delay}\right)\frac{fps}{KT} \end{aligned} \tag{3-29}$$

$$D_{trail} = \begin{cases} D_{I-trail}\ if\ \left(t_{lead} - \mathrm{t_{I-trail}}\right) \le \mathrm{t_{delay}} \\ D_{D-trail}\ if\ \left(t_{lead} - \mathrm{t_{I-trail}}\right) > \mathrm{t_{delay}} \end{cases} \tag{3-30}$$

Then, solve the D_{EAS} formula to determine the starting geometric altitude:

$$\csc\gamma\ (h - 7.31543 \times 10^{-6}\, h^2\ +\ 1.91449 \times 10^{-11}\, h^3) =\ D_{trail} \tag{3-31}$$

$$1.91449 \times 10^{-11}\, h^3 - 7.31543 \times 10^{-6}\, h^2 + h - D_{trail}\ \sin\gamma = 0 \tag{3-32}$$

The last term, D_{trail} sinγ, represents an EAS equivalent altitude, h'. Thus, the resulting solution will be a conversion from the EAS equivalent altitude (h') to the geometric altitude (h). The real cube root of the cubic formula is a complicated formula. To simplify it, the cube root is expanded into a Taylor series and the first four terms of the series are used:

$$h_{trail} = h' + 7.31543 \times 10^{-6}\, h'^2 + 8.78862 \times 10^{-11}\, h'^3 + 1.25718 \times 10^{-15}\, h'^4 \tag{3-33}$$

The X runway coordinate for the trail aircraft is then:

$$X_{trail} = -\cot\gamma\ (h_{trail} - h_{TCH}) \tag{3-34}$$

Finally, the compression length ($d_{compression}$) is:

$$d_{compression} = \min_{750}(X_{FAF} - d_{collision} - X_{trail}) \tag{3-35}$$

Using the prior example of the lead aircraft with a final approach speed of 120 KT and a trail aircraft with a final approach speed of 130 KT, the resulting value of $d_{compression}$ and intermediate terms are:

t_{lead}	= 147.4 seconds
$t_{I\text{-}trail}$	= 135.5 seconds, (t_{lead} - $t_{I\text{-}trail}$) = 11.9 seconds > t_{delay} so compute $X_{D\text{-}trail}$
t_{decel}	= 49.3 seconds
D_{trail}	= 36891 ft
h_{trail}	= 1959 ft
X_{trail}	= -36076 ft
$d_{compression}$	= 2029 ft

In comparison to the earlier example using the assumption that TAS = EAS, the compression length grew from 1957 ft to 2029 ft, a difference of 72 ft. So, how can the compression length be larger when the time of flight for both aircraft is shorter? The answer is that the trail aircraft maintains a higher altitude and, therefore, has a slightly higher true airspeed, even when the equivalent airspeed is equal to the lead aircraft. Depending on the initial separation, this effect can cause added compression that is greater than the reduced compression from the shorter flight time. It is a limitation of the EAS-based model. In the procedure, the trail aircraft uses a speed management algorithm that maintains separation through deceleration, effectively causing the trail aircraft to track the true airspeed of the lead vehicle. Therefore, until the trail vehicle decelerates to its final approach speed as an equivalent airspeed, the trail's equivalent airspeed should be slightly lower than the equivalent airspeed of the lead. There is no simple mechanism to modify the EAS-based model for this behavior. What is certain is that the compression length computed from such a modification would be between those computed by the EAS-based model and the TAS=EAS assumption. The EAS-based model often provides the more conservative estimate. Furthermore, the EAS-based model remains sufficiently simple to program or to use in generating look-up tables; therefore, it can be used in real-time by flight deck or controller systems to generate custom values of the front-gate separation for specific pairings.

This kinematic model has other simplifications that can incrementally affect results. First, the

model does not account for path deviation (lateral or longitudinal FTE) which can modify the flown distance (and therefore time) from FAF to touchdown. However, the longitudinal window in which the separation between aircraft is allowed to float (see section 3.4.3) partly accounts for the path deviation. The model also does not account for longitudinal deviation in the lead initiating the deceleration segment. Late deceleration will shorten the compression distance; early deceleration will lengthen it. The equations in this section can be adjusted to examine late or early deceleration, and this can be pursued if a future need arises for improved analysis. Lastly, the model is limited to the standard day profile for density in the 1976 atmosphere model, actual density that departs from the standard day profile will also adjust the compression distance. Again, investigating greater diversity in density profiles is left to future work if needed.

3.3. Front Gate for the Constant Speed Segment

When the lead aircraft reaches the final approach fix (FAF), the front gate is the minimum of 1500 ft (see section 3.1) or the sum of the collision-free separation at the threshold ($d_{collision}$) and the compression distance ($d_{compression}$). The previous section details the formulas used to derive $d_{compression}$ but variation of the actual airspeed to the planned airspeed was not addressed. In reality, the actual deviation of the airspeed from planned resembles a random walk plus a bias about the planned airspeed. The equations for $d_{compression}$ assume constant speed and cannot accommodate the random walk contribution to variation. However, if one assumes the random walk is approximately symmetric about the bias, then its effect on front gate position is likely to be small enough to negligible. This leaves the bias, which can be added to the planned aircraft speed. Comprehensive studies of actual vs. commanded speed over the approach path could not be found. However, Helleberg, et al. [Helleberg2006] performed an analysis of actual versus planned speed at the threshold. Unfortunately, the quantitative values presented included both manual and autothrottle flights though the study also graphically depicts separate distributions for autothrottle and manual flights. Moreover, the planned airspeed was derived from a V_{ref} lookup table after estimating the aircraft landing weight. This method is necessary to combine the manual and autothrottle flights. However, for the paired-approach, the data of interest is deviation from commanded speed with autothrottle engaged. In Helleberg's study, flights with autothrottle engaged could have commanded speeds that differ from the planned speed. Still, for the most automated aircraft models, the Airbus A320 and Boeing 777, the mean deviation of actual speed from planned was +3.24 KT and +2 KT respectively with standard deviations of 3.6 and 2.8 KT. From these numbers, it appears reasonable to assume that the bias in the actual versus planned difference in airspeed (ΔV) between the trail and lead aircraft is between 4 and 6 KT. Since the compression distance expands as the lead aircraft airspeed decreases and the trail aircraft airspeed increases, the bias is applied by decreasing the lead aircraft airspeed by half the bias and increasing the trail aircraft airspeed by half the bias.

Table 3-2 and Table 3-3 show the front gate for lead aircraft approach speeds of 100 to 140 knots equivalent airspeed (KEAS) with the trail aircraft ΔV from 0 to 20 KEAS and with a ΔV bias of 0, 4, and 6 KEAS. The values are color-coded based on the length of the front gate:

1500 ft ≤ Green ≤ 2500 ft
2500 ft < Yellow ≤ 3500 ft
3500 ft < Red ≤ 4500 ft
4500 ft < Purple

Table 3-2 presents this data for current generation aircraft and Table 3-3 presents this data for next generation aircraft.

Table 3-2: Front Gate for Current Generation Fleet

Planned V_{app} of Lead Aircraft	ΔV_{app} Variation	Planned ΔV_{app} of Trail Aircraft Final Approach Speed				
		+0 KEAS	+5 KEAS	+10 KEAS	+15 KEAS	+20 KEAS
100 KEAS	0 KEAS	1500	2315	3242	4204	5201
	+4 KEAS	2166	3104	4076	5083	6125
	+6 KEAS	2557	3518	4513	5542	6606
110 KEAS	0 KEAS	1500	2147	2995	3882	4808
	+4 KEAS	2011	2866	3759	4690	5659
	+6 KEAS	2367	3244	4159	5112	6102
120 KEAS	0 KEAS	1500	1993	2779	3608	4481
	+4 KEAS	1868	2657	3488	4362	5278
	+6 KEAS	2195	3007	3860	4755	5692
130 KEAS	0 KEAS	1500	1851	2588	3376	4214
	+4 KEAS	1735	2471	3256	4090	4972
	+6 KEAS	2039	2799	3607	4463	5366
140 KEAS	0 KEAS	1500	1719	2422	3185	4009
	+4 KEAS	1610	2307	3061	3874	4745
	+6 KEAS	1895	2618	3398	4235	5128

Table 3-3: Front Gate for Next Generation Fleet

Planned V_{app} of Lead Aircraft	ΔV_{app} Variation	Planned ΔV_{app} of Trail Aircraft Final Approach Speed				
		+0 KEAS	+5 KEAS	+10 KEAS	+15 KEAS	+20 KEAS
100 KEAS	0 KEAS	1500	2120	3060	4035	5045
	+4 KEAS	1963	2914	3899	4919	5973
	+6 KEAS	2357	3331	4339	5381	6457
110 KEAS	0 KEAS	1500	1978	2839	3739	4678
	+4 KEAS	1834	2703	3608	4552	5534
	+6 KEAS	2192	3083	4011	4976	5979
120 KEAS	0 KEAS	1500	1850	2649	3491	4377
	+4 KEAS	1717	2519	3363	4250	5178
	+6 KEAS	2047	2871	3738	4646	5595
130 KEAS	0 KEAS	1500	1734	2484	3285	4135
	+4 KEAS	1610	2360	3157	4004	4899
	+6 KEAS	1916	2690	3511	4379	5296
140 KEAS	0 KEAS	1500	1628	2344	3120	3956
	+4 KEAS	1511	2221	2989	3814	4699
	+6 KEAS	1799	2535	3328	4177	5084

The CONOPS currently identifies a minimum approach speed (V_{app}) of 120 KT and a target capability to accommodate ΔV of up to 20 KT [MITRE2013]. However, both values are identified as to-be-resolved (TBR). The tables show that for parallel, paired approach using

echelon spacing, a planned ΔV of 20 KT requires a front gate larger than 4500 ft (0.74 NM) for all speeds if actual ΔV can vary. Therefore, a planned ΔV of 20 KT appears infeasible for the paired approach. For lead aircraft with $V_{app} \geq 120$ KT, a planned $\Delta V \leq 15$ KT can be accommodated with a front gate of 4500 ft if the bias in actual ΔV can be held below 6 KT. This front gate can also accommodate slower V_{app} if planned $\Delta V \leq 10$ KT. A front gate of 3500 ft can accommodate $V_{app} \geq 120$ KT and planned $\Delta V \leq 10$ KT if the bias in actual ΔV can be held below 4 KT, which may be feasible for next generation aircraft. A front gate of 3500 ft can also handle all V_{app} and the maximum ΔV bias if planned $\Delta V \leq 5$ KT. Overall, a front gate of 2500 feet covers 31% of the table cells, a front gate a 3500 ft covers 55% of the cells, and a front gate of 4500 feet covers 77% of the cells. This study will explore the feasibility of the procedure with front gates of both 3500 ft, which might be achievable for planned $\Delta V \leq 10$ KT with future avionics, and 4500 ft, which expands the pairable ΔV to 15 KT.

3.4. The Wake-Safe Distance

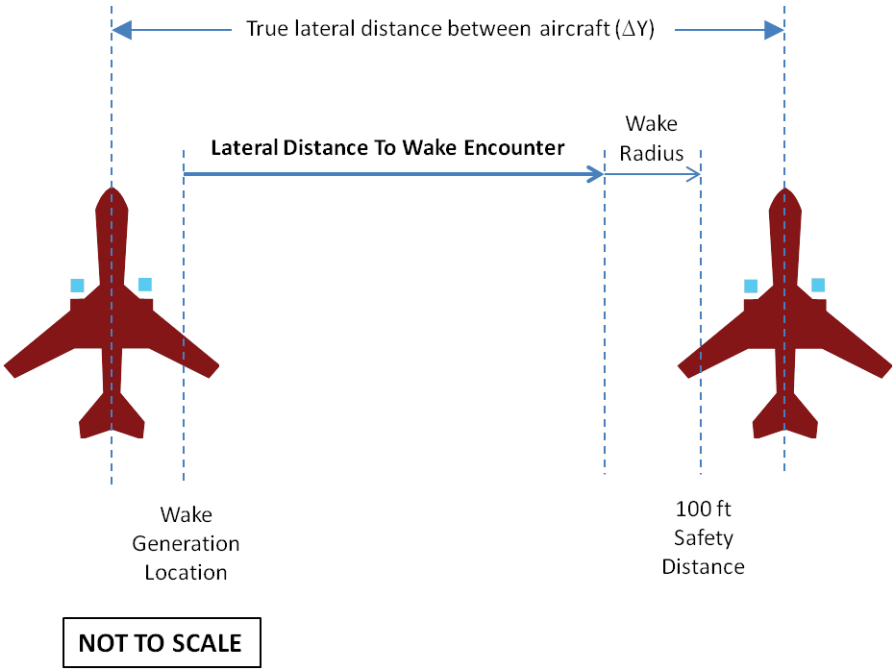

Figure 3-4: Wake Transport Model

3.4.1. Modeling Wake Transport

This study uses the wake transport model described in section A.3 of the CONOPS [MITRE2013]. The model performs a constant velocity transport of the wake from its generation point to the wake encounter zone of the trailing vehicle. The transport velocity is the sum of the crosswind velocity and, when below 400 ft AGL, a wake self-transport velocity of 2 knots. Figure 3-4 depicts the geometry that defines the distance the wake travels laterally before encountering the trailing vehicle.[2] The wake encounter zone is defined as a lateral distance from

[2] Note that Figure 3-4 shows the geometry using the instantaneous true location of each aircraft. Applying the model to a given runway separation with aircraft that perform to a given total system error is discussed later.

the centerline of the trailing vehicle. This distance is defined as a safe encounter distance of 100 feet plus the radius of the wake vortex.[3] The distance for the wake to travel is the lateral distance between its generation point and the wake encounter zone.

The following equation expresses the distance to a wake encounter:

$$D_{encounter} = \Delta Y - D_{safe} - R_{vortex} - D_{vortex} \quad (3\text{-}36)$$

where,

ΔY is the true lateral distance between aircraft, in feet.
D_{safe} is the safe encounter distance from the trail aircraft's centerline, it equals 100 ft.
R_{vortex} is the radius of the vortex which equals ($D_{vortex}/2$).
D_{vortex} is the generation location of the vortex from the lead aircraft's centerline. It is equal to ($\pi D_{wingspan}/8$) where $D_{wingspan}$ is the wingspan of the lead aircraft.

This study will assume that the lead aircraft is a Boeing 747-400.[4] The Boeing 747-400 has a wingspan of 211 ft 5 in. The distance equation, therefore, reduces to:

$$D_{encounter} = \Delta Y - 224.5\ ft \quad (3\text{-}37)$$

The next part of the problem is determining the worst-case (i.e. minimum) ΔY for the closely-spaced parallel runway (CSPR) procedure. This is discussed in the next section.

$D_{encounter}$ is then converted to a time-to-encounter ($T_{encounter}$) by dividing $D_{encounter}$ by the wake transport velocity ($V_{transport}$). $V_{transport}$ is the sum of the maximum allowable crosswind ($V_{crosswind}$) and, if under 400 ft AGL, the self-transport velocity ($V_{self\text{-}transport}$):

$$V_{transport} = V_{crosswind} + \begin{cases} V_{self-transport} & \text{if h} < 400 \text{ ft AGL} \\ 0 & \text{if h} \geq 400 \text{ ft AGL} \end{cases} \quad (3\text{-}38)$$

The CONOPS uses a "worst-case" $V_{self\text{-}transport}$ of 2 knots [MITRE2013]; however, since this study is looking at the wake-safe distance at the FAF, $V_{self\text{-}transport}$ will be zero. For $V_{crosswind}$, this study uses a worse-case value of 10 knots.

Lastly, the longitudinal wake-free boundary is the product of the time-to-encounter ($T_{encounter}$) and the trail aircraft's true speed (V_{trail}).

$$L_{wake-free} = T_{encounter} * V_{trail} = D_{encounter} * \frac{V_{trail}}{V_{transport}} \quad (3\text{-}39)$$

3.4.2. Closest Lateral Separation under Normal Operations

The closest allowable lateral separation under normal operations (ΔY) determines the

---

[3] The safe encounter distance is not the distance that avoids the wake but the distance where a wake encounter does not endanger the aircraft. This distance is used to maintain consistency with the analysis presented in the CONOPS [MITRE2013]. However, in future studies, replacing the safe encounter distance with the half-wingspan of the largest trail aircraft is recommended. This changes the runway separation calculated by the difference between the half-wingspan and 100 ft.

[4] The Boeing 747-400 was chosen to maintain consistency with the CONOPS [MITRE2013]. Prior NASA studies have used the wider Boeing 747-8.

design-to, wake-free boundary for the procedure. The lateral separation between aircraft during the procedure is determined by the actual path each aircraft flies. The deviation of the actual path from the desired path is characterized by the total system error (TSE). TSE is made of three error components: path definition error (PDE), navigation error (NE), and flight technical error (FTE). PDE is the difference between the path defined by the on-board avionics and the desired path; it is normally negligible and can be ignored. NE is the error between the position of the aircraft estimated by the on-board navigation system and its actual position. FTE is the error in the autopilot or crew's ability to fly the path. NE and FTE are both modeled by a normal distribution; therefore, TSE is also modeled as a normal distribution. The TSE, NE, and FTE values presented here are 95% confidence bounds (1.96σ).

To date, comprehensive studies of FTE for aircraft on approach have examined a mixture of hand-flown and autopilot approaches using the Instrument Landing System (ILS) as the primary navigation aid. Thomas and Timoteo [Thomas1990] and Thomas, Timoteo, and Huang [Thomas1993] showed that the FTE of ILS approaches increases with distance from threshold. FTE exceeded 200 ft at distances greater than 8 to 10 NM from the threshold and, on final approach, FTE was less than 40 ft/NM from threshold. Eckstein [Eckstein2011] also depicted the localizer deviation of ILS approaches starting at 7 NM from threshold and computed the FTE at a point 3 NM from the threshold. Unlike previous work, Eckstein divided the data between hand-flown and autopilot approaches. The FTE of hand-flown approaches was an order of magnitude greater than autopilot approaches. The FTE of the autopilot approaches was less than 10 feet. Eckstein's study keeps open the possibility that it may be possible for the paired approach procedure to be performed from start to finish using only the ILS with the autopilot engaged. However, until a comprehensive analysis of autopilot only approaches with ILS have been conducted, this study will proceed under the assumption that the aircraft pair performs an RNP or GPS RNAV approach to the FAF (though each aircraft may transition to the ILS navaid afterwards). This study uses two sources of TSE or FTE data for RNAV or RNP approach to represent current generation and next generation aircraft. Murphy presented data from Air France showing that the TSE of aircraft on RNP approach was 59 m (194 ft) at the time they disengaged the autopilot [Murphy2010]. Passerini provides data on the Quantas fleet of Boeing 737-800s that measure the FTE of RNP approaches at 0.02 NM (37 m or 122 ft) [Passerini2011]. The TSE value of 59 m will be used to represent RNP or RNAV performance in the current generation aircraft. The FTE value of 37 m will be used to represent next generation aircraft.

This study assumes that a GPS-based navigation system or equivalent will be used to estimate the position of the aircraft. Current generation aircraft are assumed to have an autonomous GPS system. RTCA DO-242A Appendix J.3.3 characterizes the lateral NE of autonomous GPS as 12.5 m; however, in an unpublished work used for development of the CONOPS, Eftekari [Eftekari 2008] identifies the lateral NE of autonomous GPS as 8 m (26 ft) based on observations from ADS-B flight tests at the FAA Technical Center in July 2007. This study will use the smaller 8 m NE. Next generation aircraft are assumed to have a Wide-Area Augmentation System (WAAS) GPS system or better. RTCA DO-242A Appendix J.3.3 characterizes WAAS GPS with a lateral NE of 3.5 m (12 ft) [RTCA2002].

Table 3-4: Total System Error of Aircraft Fleets

	TSE	FTE	NE	Event Duration	Events/Procedure
Current Generation	59.0 m	58.5 m	8.0 m	70 s	6
Next Generation	37.2 m	37.0 m	3.5 m	70 s	6

The final TSE, FTE, and NE values are summarized in Table 3-4. Recognize that these errors are defined for a sample. To ascertain their affect on the maximum deviation over the entire approach path during normal operations, it is necessary to determine how many samples will occur during the course of the procedure. Aircraft do not suddenly jump from one error to the next, the error occurs as a random walk with a period in distance or time. Boeing identifies the period between independent FTE events at 70 seconds [Boeing2012]. For GPS receivers, the period between independent navigation error events is four to eight minutes. However, because NE is much smaller than FTE, the period of NE events is made equal to FTE events for simplicity. Thus, the period of independent events for TSE, FTE, and NE are each set at 70 seconds for both current and next-generation aircraft. The paired-approach procedure can have a duration of up to six minutes at KSFO based on approach path geometry and speed schedule. Therefore, six independent events can occur during the course of the procedure.

Having established the lateral error characteristics of the aircraft, these characteristics are applied to a definition of normal operation in order to determine the bounds on lateral deviation. Normal operation is defined by the alert rate and alert integrity for the participating aircraft. Independent monitoring of the lead aircraft by the trail is not practical because ADS-B uncertainties are large relative to the lateral path separation (see section 3.4.3). Therefore, each aircraft is responsible for monitoring its own lateral deviation. Aircraft are capable of monitoring their lateral FTE directly. The alert rate is assumed to be 10^{-4} alerts per aircraft per procedure without a blunder. Because lateral FTE is being monitored but lateral NE cannot be monitored. The aircraft can exceed its alerting bounds without an alert. Therefore, the containment bound for normal operation is also defined by an alert integrity criterion equivalent to RNP integrity requirements of 99.999% containment per hour.

First, the alerting bounds are computed. Part of the per-aircraft, per-procedure alert rate ($ar_{aircraft}$) is allocated to alerted hardware failure ($ar_{avionics}$) and part of this rate is allocated to aircraft performance (ar_{FTE}). It is assumed that the hardware will have an alerted failure at a rate of 5 x 10^{-5}/hr. This alerted failure rate is taken from the continuity requirement for RNP of 99.99% per hour and assumes that half the probability of continuity failure is due to alerted hardware failure. It is also assumed that the hardware alert rate is linear with time and reduces to $ar_{avionics}$ = 5 x 10^{-6}/procedure. The remaining alert rate due to aircraft performance is 9.5 x 10^{-5} per procedure. The equivalent alert rate per FTE sample (ar_{FTE}) is given by Equation 3-41 where n_{FTE} is the number of FTE samples per procedure. This equation is derived from the probability of no alert (1 - $ar_{aircraft}$) being equal to the combined probability of no hardware failure (1 - $ar_{avionics}$) and the probability that the aircraft will not exceed the alerting bound (1 - ar_{FTE}) for each of the six FTE samples (Equation 3-40). The resulting per FTE sample alert rate is 1.6 x 10^{-5}.

$$\left(1 - ar_{aircraft}\right) = (1 - ar_{avionics})(1 - ar_{FTE})^{n_{FTE}} \tag{3-40}$$

$$ar_{FTE} = 1 - \left(\frac{1 - ar_{aircraft}}{1 - ar_{avionics}}\right)^{1/n_{FTE}} \tag{3-41}$$

Using ar_{FTE}, the FTE bound that triggers an alert is determined from the normal distribution. Though deviations to only one side of the aircraft adversely affect the lateral separation between aircraft, the FTE bound will be computed for alerting on either side of the aircraft path. This is simpler from a procedural perspective. There is no need to identify the aircraft as being on the left or right runway and the alerting remains similar to loss of containment alerts for RNP. The following equation computes the alerting bound (y_{alert}) where erf^{-1} is the inverse error function:

$$y_{alert} = \frac{FTE}{1.96}\sqrt{2}\, erf^{-1}(2\, ar_{FTE} - 1) \tag{3-42}$$

Next, the alert integrity bound is computed. This bound is designed to be equivalent to the RNP requirement of 99.999% containment per hour per aircraft, i.e. $up_{aircraft} = 10^{-5}$ / hr. The study assumes that integrity loss is divided equally between un-alerted hardware failure ($up_{avionics}$) and position uncertainty (up_{TSE}). Therefore, both contributions have a probability of 5 x 10^{-6} / hr. This probability is further reduced to a probability of $up_{avionics} = up_{TSE} = 9.7 \times 10^{-8}$ per FTE sample. The resulting probability of un-alerted containment loss during the procedure (accounting for both aircraft) is 1.75 x 10^{-6}.

The quantity up_{TSE} represents the probability that the true position of aircraft (y_{true}) is beyond the integrity bound ($y_{integrity}$) when the aircraft does not generate an alert. This occurs when the navigation error is of a sufficient adverse value to place the estimated position of the aircraft (y_{FTE}) below the alerting bound y_{alert}. Because of the symmetry in the normal distribution of lateral deviation, up_{TSE} can be formulated as twice the probability, on one side of the path, that y_{true} will be outside $y_{integrity}$ when $|y_{FTE}| < y_{alert}$. Thus, one constructs the combined probability that the navigation error (y_{NE}) is greater than $y_{integrity} - y_{FTE}$ for all y_{FTE} in the range $[-y_{alert}, y_{alert}]$. This is represented by the dual integral below:

$$up_{TSE} = 2\int_{-y_{alert}}^{y_{alert}}\int_{y_{integrity}-y_{FTE}}^{\infty}\left(\frac{e^{-\frac{y_{FTE}^2}{2\,\sigma_{FTE}}}}{\sqrt{2\,\pi}\,\sigma_{FTE}}\right)\left(\frac{e^{-\frac{y_{NE}^2}{2\,\sigma_{NE}}}}{\sqrt{2\,\pi}\,\sigma_{NE}}\right) dy_{NE}\, dy_{FTE} \tag{3-43}$$

where σ_{FTE} and σ_{NE} are the standard deviation of the FTE and NE errors, respectively. Recognizing that the inner integral is equivalent to an integral with the range $[-\infty, y_{FTE} - y_{integrity}]$, the double integral reduces to:

$$up_{TSE} = 2\int_{-y_{alert}}^{y_{alert}}\left(\frac{\left(e^{-\frac{y_{FTE}^2}{2\,\sigma_{FTE}}}\right) erf\left(\frac{y_{integrity} - y_{FTE}}{\sqrt{2}\,\sigma_{NE}}\right)}{2\sqrt{2\,\pi}\,\sigma_{FTE}}\right) dy_{FTE} \tag{3-44}$$

where *erf*() is the error function. This outer integral cannot be further reduced and must be resolved numerically. Therefore, the $y_{integrity}$ value that corresponds with a up_{TSE} value is solved iteratively using root-finding methods.

The design-to lateral separation bounds for each aircraft are the larger of y_{alert} and $y_{integrity}$. Table 3-5 summarizes the probabilities used to define normal operation in this section. Table 3-6 shows the values of σ_{FTE}, σ_{NE}, y_{alert} and $y_{integrity}$, rounded up to the nearest foot, for current and next generation aircraft and how these values affect required path separation. The required path separation is computed from Equation 3-37 where $\Delta Y = 2 \times \max(y_{alert}, y_{integrity})$, i.e. the worst case is when both aircraft deviate toward each other by the design-to separation bounds. The path separation values shown here merely depict the spacing at which the wake vortex does not need to move to encounter the trail aircraft if both aircraft are positioned at their integrity bounds. A feasible runway spacing must be much greater than the value shown. These results show that neither current nor next generation aircraft can accommodate 750 ft runway spacing with a parallel echelon procedure. The question is how much spacing is needed to enable the procedure.

To answer this question it is necessary to determine the length of the echelon window based on expected longitudinal deviation during normal operation.

Table 3-5: Summary of Probabilities Defining Normal Lateral Deviation

Total Alert Rate ($ar_{aircraft}$)	10^{-4} / aircraft / procedure
Hardware Alert Rate ($ar_{avionics}$)	5 x 10^{-6} / procedure
Position Alert Rate (ar_{FTE})	9.5 x 10^{-5} / procedure
	1.583 x 10^{-5} / FTE sample
Total Un-alerted Lateral Containment Loss ($up_{procedure}$)	2.3 x 10^{-6} / procedure
Loss due to un-alerted hardware failure ($up_{avionics}$)	5.8 x 10^{-7} / procedure
	9.7 x 10^{-8} / FTE sample
Un-alerted loss due to position uncertainty (up_{TSE})	5.8 x 10^{-7} / procedure
	9.7 x 10^{-8} / FTE sample
Number of FTE samples per procedure (n_{FTE})	6
Duration of FTE sample	70 seconds

Table 3-6: Lateral Deviation Parameters under Normal Operation

	Current Generation	Next Generation
σ_{FTE}	98 ft	62 ft
σ_{NE}	13.4 ft	5.9 ft
y_{alert}	408 ft	258 ft
$y_{integrity}$	438 ft	271 ft
path separation	>> 1100 ft	>> 767 ft

3.4.3. Minimum Longitudinal Window under Normal Operations

The minimum longitudinal window during normal operations is defined similarly to the expected lateral deviation during normal operations in the previous section. Normal operation is defined by a desired alert rate and an alert integrity criterion similar to lateral operation. Here, the trail aircraft monitors its position relative to the lead aircraft and attempts to maintain a desired separation. As with lateral monitoring, the desired alert rate is to be no greater than 10^{-4} per procedure. Alert integrity due to position uncertainty will also be maintained to the same requirement as RNP integrity.

One difference in the longitudinal monitoring is that the longitudinal separation is subject to both ADS-B OUT errors of lead aircraft and the longitudinal TSE of both aircraft. Longitudinal TSE and its component FTE and NE are assumed equal to the lateral TSE, FTE, and NE. The same similarity holds for the duration of a longitudinal TSE event (70 seconds) and the number of longitudinal TSE events in a procedure (6). ADS-B OUT data is assumed to be derived from the lead aircraft's navigation solution. Therefore, the variation in ADS-B reported position has three components, navigation error (NE), latency compensation error, and uncompensated latency error. The latter two are combined into an ADS-B latency error (ALE). The combination of all three components is the estimated position uncertainty (EPU) of the ADS-B output. ADS-B EPU is normally reported as a 2-D radius uncertainty and is assumed to conform to a Rayleigh distribution. Therefore, the standard deviation of uncertainty in longitudinal position (σ_{EPU}) is EPU/2.447. Current Generation aircraft are assumed to have an EPU of 92.6 m, which conforms to the FAA ADS-B rule [FAA2010]. Next Generation aircraft are assumed to have an EPU of 10

m associated with a Navigation Accuracy Category for Position (NACp) value of 10. These errors are used to determine the variation in observed separation to the planned separation. The observed separation is the difference in the observed position of the lead aircraft (via ADS-B OUT) and the observed position of the trail aircraft (via its navigation system). The ADS-B OUT report represents the lead aircraft's observation of its own longitudinal FTE plus the ALE. The trail aircraft uses observation of its own position to monitor its longitudinal flight technical error (FTE). Therefore, the variation in observed longitudinal separation is a combination of both aircraft's FTE and the ALE of the lead aircraft:

$$\sigma_{obs} = \sqrt{(\sigma_{FTE})^2_{lead} + (\sigma_{FTE})^2_{trail} + (\sigma_{ALE})^2_{lead}} \tag{3-45}$$

The standard deviation of ALE is computed by subtracting the contribution of NE to EPU:

$$\sigma_{ALE} = \sqrt{\sigma^2_{EPU} - \sigma^2_{NE}} \tag{3-46}$$

The longitudinal alert uses similar probability assumptions to the lateral alert. The longitudinal alert rate is 10^{-4} per procedure with alerted hardware failures occurring with a probability of 5 x 10^{-6} / procedure. Therefore, alerts due to separation performance (ar_{sep}) are 9.5 x 10^{-5} / procedure or 1.583 x 10^{-5} / FTE sample. There are two contributors to variation in separation performance. The first is the variation in observed separation. The second is the response time (t_{delay}) of the trail aircraft to the lead aircraft. During that time, the airspeed difference between the two aircraft can vary. For this study, the longitudinal airspeed difference is assumed to vary with a standard deviation ($\sigma_{\Delta V}$) of 3.4 KT (5.7 ft/s or 1.7 m/s); this number is derived from an assumed 3 KT standard deviation in the horizontal airspeed of each aircraft. The equivalent spacial variation ($\sigma_{\Delta x}$) is the product of t_{delay} and $\sigma_{\Delta V}$. For current generation aircraft, $\sigma_{\Delta x}$ is 29 ft and, for next generation aircraft, $\sigma_{\Delta x}$ is 20 ft. Therefore the total variation in separation performance (σ_{sep}) is:

$$\sigma_{sep} = \sqrt{\sigma^2_{obs} + \sigma^2_{\Delta x}} \tag{3-47}$$

The longitudinal alerting bound (x_{alert}) is therefore:

$$x_{alert} = \sigma_{sep}\sqrt{2}\, erf^{-1}(2\, ar_{sep} - 1) \tag{3-48}$$

The integrity of the longitudinal alert also uses similar probability assumptions to the lateral alert. Un-alerted longitudinal containment loss is 10^{-5} / hr with the contributions of un-alerted hardware failure ($up_{avionics}$) and position uncertainty (up_{TSE}) both at 9.7 x 10^{-8} per FTE sample. Derivation of the integrity bound ($x_{integrity}$) is the same as for the lateral integrity bound with the following differences. The two PDFs involved are the PDF of separation performance (and thus a function of σ_{sep}) and the PDF of navigation uncertainty. However, the navigation uncertainty in this case is the combined navigation uncertainty of the two aircraft. Since the navigation uncertainty of the two aircraft is assumed equal, the PDF of the combined navigation uncertainty is a function of $\sqrt{2}\ \sigma_{NE}$. The resulting equation for $x_{integrity}$ is:

$$up_{TSE} = 2\int_{-x_{alert}}^{x_{alert}} \left(\frac{\left(e^{-\frac{x_{sep}^2}{2\,\sigma_{sep}}} \right) erf\left(\frac{y_{integrity} - y_{FTE}}{2\,\sigma_{NE}} \right)}{2\sqrt{2\,\pi}\,\sigma_{sep}} \right) dx_{sep} \tag{3-49}$$

The design-to longitudinal window for the trail aircraft (x_{window}) is double the larger of y_{alert} and $y_{integrity}$. Table 3-7 summarizes the probabilities used to define normal operation in this section. Table 3-8 shows the values of σ_{sep}, σ_{NE}, x_{alert}, $x_{integrity}$, and x_{window}, rounded up to the nearest foot, for current and next generation aircraft.

Table 3-7: Summary of Probabilities Defining Normal Longitudinal Deviation

Total Alert Rate ($ar_{aircraft}$)	10^{-4} / procedure
Hardware Alert Rate ($ar_{avionics}$)	5 x 10^{-6} / procedure
Position Alert Rate (ar_{FTE})	9.5 x 10^{-5} / procedure
	1.583 x 10^{-5} / FTE sample
Total Un-alerted Lateral Containment Loss ($up_{procedure}$)	1.17 x 10^{-6} / procedure
Loss due to un-alerted hardware failure ($up_{avionics}$)	5.8 x 10^{-7} / procedure
	9.7 x 10^{-8} / FTE sample
Un-alerted loss due to position uncertainty (up_{TSE})	5.8 x 10^{-7} / procedure
	9.7 x 10^{-8} / FTE sample
Number of FTE samples per procedure (n_{FTE})	6
Duration of FTE sample	70 seconds

Table 3-8: Longitudinal Deviation Parameters under Normal Operation

	Current Generation	Next Generation
σ_{sep}	194 ft	97 ft
σ_{NE}	13.4 ft	5.9 ft
x_{alert}	806 ft	403 ft
$x_{integrity}$	842 ft	418 ft
x_{window}	1684 ft	836 ft

3.4.4. Calculating the Wake-Safe Distance

The required wake-safe distance ($L_{wake\text{-}free}$) is a simple summation of the longitudinal window (x_{window}) and the front-gate ($x_{front\text{-}gate}$):

$$L_{wake-free} = x_{front-gate} + x_{window} \tag{3-50}$$

3.5. Determining Feasible Runway Separation and Conclusions

The feasible runway separation can be computed as a function of the required wake-safe distance ($L_{wake\text{-}free}$) and the lateral integrity ($y_{integrity}$). First, the required wake transport distance ($D_{encounter}$) is computed by inverting Equation 3-39:

$$D_{encounter} = L_{wake-free} \frac{V_{transport}}{V_{trail}} \quad (3\text{-}51)$$

Before the FAF, the worst-case wake transport velocity ($V_{transport}$) is equal to the maximum adverse crosswind of 10 KT. The trail aircraft velocity (V_{trail}) is nominally 180 KT but we will assume that variation in speed performance can decrease it to a minimum of 177 KT. With $D_{encounter}$ computed, the minimum runway separation (ΔY_{runway}) that is feasible for the procedure is:

$$\Delta Y_{runway} = 224.5\, ft + D_{encounter} + 2\, y_{integrity} \quad (3\text{-}52)$$

Table 3-9 shows the results, rounded up to the nearest foot, for current and next generation aircraft:

Table 3-9: Feasible Separation Geometry

	Current Generation		Next Generation	
$x_{front\text{-}gate}$	3500 ft	4500 ft	3500 ft	4500 ft
$L_{wake\text{-}free}$	5184 ft	6184 ft	4336 ft	5336 ft
$D_{encounter}$	293 ft	350 ft	245 ft	302 ft
ΔY_{runway}	1393 ft	1450 ft	1010 ft	1066 ft

As the results show, current generation aircraft cannot conduct paired approaches on parallel paths using echelon spacing on runways less than ~1400 ft apart and next-generation aircraft cannot conduct the paired approach on runways less than ~1050 ft apart. In both cases, the minimum spacing increases by about 50 feet if the front gate must be 4500 ft at the FAF. These runway separations are the same as in the initial estimates for which passing becomes safe using the SAPA procedure (see Section 2.1.3.1). Therefore, for parallel approaches, the paired-approach with echelon spacing does not offer an increase in airports where the procedure is feasible. Furthermore, since the SAPA approach allows passing, SAPA can more easily accommodate larger differences in approach speed and lower minimum approach speeds. However, the echelon spacing approach should maintain a cost advantage for new or modified equipage since it requires only monitoring of lateral and longitudinal bounds while SAPA requires an alerting algorithm and an automated escape maneuver. Nevertheless, the above analysis used a simple wake transport model and the feasible runway separation for echelon spacing may grow if higher-fidelity models further constrict the wake-free distance. Such a case would further tilt in favor of SAPA over echelon spacing.

What aircraft performance would be necessary to enable operation at runways separated by 750 ft? Runway separation has the most sensitivity to the FTE of the participating aircraft. The FTE of the next generation aircraft was reduced until the runway separation fell at or below 750 feet for both front gates of 3500 and 4500 ft. Table 3-10 shows the results:

Table 3-10: Performance Required to Enable Paired-Approach for 750ft Runway Spacing

$x_{front\text{-}gate}$	3500 ft	4500 ft
FTE (95%)	63 ft (19.2 m)	50 ft (15.3 m)
y_{alert}	134 ft	107 ft
$y_{integrity}$	148 ft	122 ft
x_{alert}	255 ft	228 ft
$x_{integrity}$	271 ft	245 ft
$L_{wake\text{-}free}$	4042 ft	4989 ft
$D_{encounter}$	229 ft	282 ft
ΔY_{runway}	749 ft	749 ft

As the table shows, aircraft FTE must decrease by half in next generation aircraft to open the paired approach procedure for 750 foot runway spacing. The feasibility of achieving such performance on a straight approach from loss of vertical separation to the threshold is questionable. However, aircraft performing CAT IIIB ILS approaches routinely achieve this level of performance within the inner marker where the ILS navigation error is similar to the assumed WAAS GPS navigation error of 3.5 m lateral. Nevertheless, many aspects of flight within the inner marker (including airspeed and winds) are more favorable to controlling path deviation than flight beyond the FAF (outer marker). More data on actual straight-in approaches using state-of-the-art autopilot and autothrottle systems will be needed to better characterize the total system error that can be routinely achieved.

One final note, the alerting rates in this analysis are cumulative. With each aircraft having a 10^{-4} rate of lateral alerts and the trail aircraft having a 10^{-4} rate of longitudinal separation alerts, the total breakout rate for the procedure is approximately 3 in 10,000 procedures. Any further decrease in this total will require wider runway spacing or improved aircraft path performance.

4. Towards Lower Visibility Minima

The MITRE echelon procedure [MITRE2013] takes advantage of an offset leg that merges about 1 NM from the runway threshold. This is necessary so that the final 1 NM parallel landing can be achieved using VFR rules. In this section we consider the potential of an IFR landing if the ALAS algorithm were used. In our earlier work, we found that the aircraft could not be allowed to pass each other for a runway spacing of 750 ft. But there are two reasons why the ALAS alerting algorithm may enable lower visibility minima when used in conjunction with the MITRE echelon concept:

1. The total system error (TSE) is significantly smaller for the last 1 NM of the approach and therefore the ALAS alerting algorithm will be more effective here.

2. The MITRE procedure constrains the aircraft to be longitudinally separated at the FAF which will provide some longitudinal separation at the merge point even after much ground speed compression.

The tAlas simulation was configured to simulate the parallel landing after the merge point:

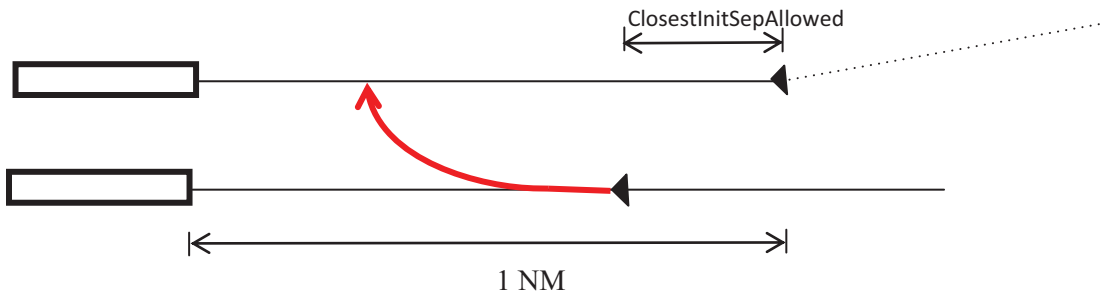

Figure 4-1: Parallel landing after the merge point

Different simulations were run varying the parameter ClosestInitSepAllowed over range from 0 ft to 250 ft and varying the parameter maximumGsDifferential over range from 0 KT to 30 KT.

Because these simualtion runs begin after the turn, they are equally valid for echelon spacing on parallel approaches.

4.1. Experimental Results Using Monte Carlo Simulation Starting 1 NM From Runway

The tAlas simulation was run in Monte Carlo mode varying runway separations, initial separation longitudinally, and the maximum ground speed difference. In all cases the intruder and ownship were given starting positions in the range of 1 NM to 1.5 NM.

We begin with a baseline result obtained by running the tAlas simulation with alerting and the escape maneuver disabled. In this simulation, the ownship was always in the rear position. The results are given in Table 4-1. Note that acceptable probabilities are indicated in blue font and unacceptable probabilities are indicated in red.

Table 4-1: Results for 750 ft Runway Spacing, No Escape Maneuver

Initial Longitudinal Separation (at 1 NM)	Max GS Difference	Probability
250 ft	5	2.34E-02 ± 4.78E-05
250 ft	10	3.65E-02 ± 5.93E-05
250 ft	15	4.49E-02 ± 6.55E-05
250 ft	20	5.00E-02 ± 6.89E-05
500 ft	5	1.63E-03 ± 1.27E-05
500 ft	10	1.18E-02 ± 3.42E-05
500 ft	15	2.33E-02 ± 4.77E-05
500 ft	20	3.15E-02 ± 5.53E-05
750 ft	5	4.38E-07 ± 1.48E-07
750 ft	10	7.40E-04 ± 8.60E-06
750 ft	15	7.01E-03 ± 2.64E-05
750 ft	20	1.52E-02 ± 3.87E-05
1250 ft	5	4.38E-07 ± 1.48E-07
1250 ft	10	4.38E-07 ± 1.48E-07
1250 ft	15	8.38E-07 ± 2.49E-07
1250 ft	20	5.87E-04 ± 7.66E-06
1500 ft	5	4.38E-07 ± 1.48E-07
1500 ft	10	4.38E-07 ± 1.48E-07
1500 ft	15	4.38E-07 ± 1.48E-07
1500 ft	20	3.34E-06 ± 5.58E-07

The largest ground speed differential for each initial longitudinal separation is given in Table 4-2.

Table 4-2: Summary of Results for 750 ft Runway Spacing, No Escape Maneuver

Initial Longitudinal Separation (at 1 NM)	Largest GS Difference that meets Target Probability
250 ft	---
750 ft	5
1250 ft	15
1500 ft	20

Clearly, without an alerting algorithm and an escape maneuver, there must be an initial longitudinal separation of at least 1500 ft at the merge point to accommodate ground speed

differences up to 20 KT. This is achieved procedurally in the MITRE concept of operations by constraining the aircraft to be 4000+ ft apart longitudinally at the FAF and disallowing pairings with large ground speed differences.

We next explored the potential of deploying the ALAS alerting algorithm on the final leg of the approach that begins 1 NM from the runway threshold. In these runs we have constrained the samples so that the ownship was always in the rear position. We note that the ALAS runway conformance algorithm could be used during the offset approach, but the full collision algorithm would likely generate a large number of false alarms while one aircraft was on the offset leg.

In Table 4-3 we show the impact of the ALAS algorithm when used on this final leg.

Table 4-3: Summary of Results for 750 ft Runway Spacing (Final Parallel Leg)

Initial Longitudinal Separation	Max GS Difference	Probability	Minimum Distance (ft)
0 ft	5	4.38E-07 ± 1.48E-07	287.91
0 ft	10	5.38E-07 ± 1.79E-07	237.37
0 ft	15	5.38E-07 ± 1.79E-07	264.17
0 ft	20	6.38E-07 ± 2.05E-07	291.13
250 ft	5	4.38E-07 ± 1.48E-07	287.91
250 ft	10	5.38E-07 ± 1.79E-07	264.17
250 ft	15	5.38E-07 ± 1.79E-07	246.49
250 ft	20	5.38E-07 ± 1.79E-07	291.13

The ALAS alerting system is especially effective here because the total system error is smaller nearer the runway.

The results are very promising but they critically depend upon having both a turn and vertical acceleration in the escape maneuver. Also, the analysis assumes that the turn of the ownship from the offset path to the centerline doesn't increase the TSE in the final 1 NM. In the next section we explore the impact of disabling the turn component of the escape maneuver.

4.2. A Closer Look at the SAPA Escape Maneuver When Near to the Ground

In this section we will provide a limited look at the problem of executing the escape maneuver when the aircraft is very near to the ground. Because of near ground obstacles, we could imagine that below a certain altitude, the aggressive turn component of the escape maneuver must be turned off, and only the vertical climb will be allowed to occur. We ran the tAlas simulation for a 1050 ft runway separation for the SAPA procedure. We turned off the turn component at different altitudes and measured the collision probability.

In Table 4-4 we present the probability of a collision as a function of the cutoff altitude where the turn component of the escape maneuver is disengaged.

Table 4-4: Simulation Runs for 1050 ft Runway using Escape Maneuver with No Turn

Cutoff Altitude (ft)	ADS-B Latency (s)	Probability (400 ft)	Probability (large cylinder)	Minimum Distance (ft)
0	1.5	9.84E-06 ± 9.81E-07	4.38E-07 ± 1.48E-07	316.55
50	1.5	1.99E-05 ± 1.40E-06	1.44E-06 ± 3.49E-07	163.95
100	1.5	2.00E-04 ± 4.47E-06	1.27E-05 ± 1.12E-06	128.78
200	1.5	1.64E-03 ± 1.28E-05	9.71E-05 ± 3.11E-06	123.07
300	1.5	3.72E-03 ± 1.92E-05	2.15E-04 ± 4.64E-06	119.49

The results are drastically different than those obtained with the turn component included. The reason for this difference is seen in the following failure case. Here, the blunder occurs near the ground (below 300 ft) and the turn component of the escape maneuver was disabled and therefore the horizontal view shows the ownship continuing to follow the centerline.

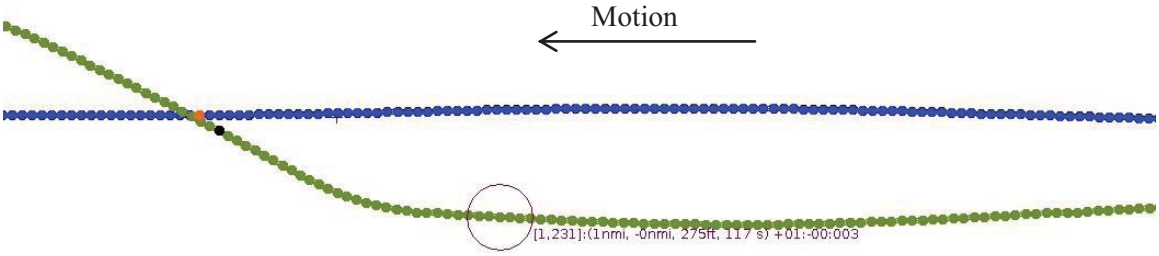

Figure 4-2: Escape maneuver near the ground (Top View)

The vertical view shows that the intruder levels out and by the time the alert occurs and the climb maneuver engages, the ownship is well below the intruder. The ownship then climbs back through the path of the intruder.

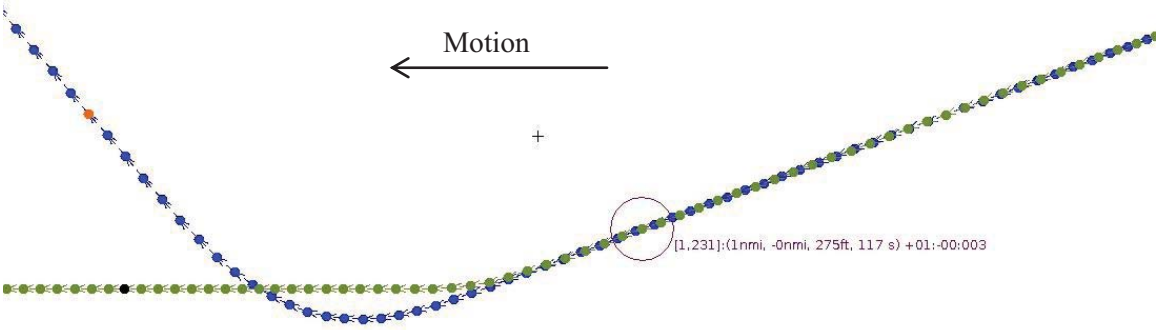

Figure 4-3: Escape maneuver near the ground (Side View)

In this trial, the blunder started at time 117 (marked by circle) and the red alert occurred 3.0 seconds later. The point of closest approach is colored in orange which occurred at time 131.5. The ownship aircraft performed a vertical climb, but no turn because the blundering aircraft was

currently located at 275 ft AGL. In this case the blunder was a level-out blunder and was slightly above the ownship. By the time the ownship maneuvers, it descends below the level out altitude of the intruder and then climbs back up into a loss of separation: (H: 232.95 ft, V: 86.75 ft). If the turn were enabled, a loss of separation would not have occurred here.

4.3. A First Look at an Intelligent Escape Maneuver

The escape maneuver examined in the previous subsection is clearly inadequate. However, an escape maneuver that is different depending on the available ownship and traffic state vectors may be able to remedy the problem. There are many avenues to pursue, but the following two approaches may be a part of the solution:

1. Use the throttle to increase ground speed rather than altitude for a short time.

2. Delay the vertical climb until sufficient horizontal separation has been achieved.

This strategy is only used when the intruder is longitudinally close to the ownship and the intruder is above the ownship in altitude. We have performed some very preliminary simulations where a ground speed acceleration of 4 m/s^2 used in conjunction with a delayed vertical ascent. This alternate maneuver was only used when the intruder was longitudinally within 350 ft and at least 20 ft above the ownship in altitude. The ground speed acceleration continues until 250 KT was reached. The vertical climb was delayed about 8 seconds.

The table shows that if the turn was not disengaged until 100 ft AGL, then this strategy has a good potential of working. In future work, we will look for ways to improve the intelligent escape maneuver further and perhaps raise the altitude further where the turn component can be turned off.

Table 4-5: Simulation Runs for 1050 ft Runway using Intelligent Maneuver with No Turn

Cutoff Altitude (ft)	ADS-B Latency (s)	Probability (400 ft)	Probability (large cylinder)	Minimum Distance (ft)
0	1.5	9.84E-06 ± 9.81E-07	4.38E-07 ± 1.48E-07	316.55
50	1.5	1.02E-05 ± 1.00E-06	5.38E-07 ± 1.79E-07	200.30
100	1.5	4.50E-05 ± 2.12E-06	2.44E-06 ± 4.71E-07	150.96
150	1.5	2.63E-04 ± 5.13E-06	1.38E-05 ± 1.17E-06	150.96
200	1.5	7.20E-04 ± 8.48E-06	3.76E-05 ± 1.93E-06	140.87
300	1.5	1.86E-03 ± 1.36E-05	9.65E-05 ± 3.10E-06	134.27

4.4. Modifying the Offset Paired-Approach to Enable Lower Decision Minima

The offset paired approach in the CONOPS is currently defined at KSFO with a minimum descent altitude (MDA) of 363 MSL (350 AGL) and a decision height (DH) of 200 ft (CAT I). This work looked at the modifications to the offset paired approach that would enable CAT II or CAT III A/B approach minima. The instrument landing system (ILS) remains the only operational technology in the near term to enable CAT II or CAT III A/B approaches. Therefore, this study examined the path stability of the trail aircraft at heights of 200 ft, 100 ft, and 50 ft AGL after the aircraft turned onto the extended runway centerline to capture the localizer. The

intercept point of the offset path with the extended centerline was varied and set at heights along the glidepath of 370 ft, 587 ft, 730 ft, and 833 ft. The first intercept height is 1 NM from the threshold and allows the fastest aircraft to turn onto the centerline above the 200 ft DH. The heights in between approximately correspond to turns completed by the slowest aircraft at distances of 1 NM and 1.5 NM from the 200 ft DH. The 833 ft height is the highest intercept height that allows the fastest aircraft to initiate the turn onto centerline after the stabilized approach point (SAP).

The high-fidelity transport-class aircraft simulation in Langley's Cockpit Motion Facility (CMF) was used to assess the FTE of aircraft at each of the decision heights. To perform a Monte-Carlo analysis with the high-fidelity simulation, it was necessary to configure the flight automation differently from the expected procedure design but try to maintain similar lateral deviation errors. In the modified offset paired-approach procedure, the trail aircraft is expected to fly the offset path as an RNP or RNAV(GPS) leg as described in the CONOPS. This offset path is automated by the flight management computer (FMC). The FMC then executes the turn from the offset leg onto the centerline. When the turn nears completion, the localizer and approach modes will be armed either manually by the crew or automatically by the FMC (which may require equipage modifications). The crew will then manage the flight in accordance with procedures for CAT I, CAT II, CAT IIIA, or CAT IIIB approach as normal. The CMF simulation utilizes a hardware FMC; therefore, it is not practical to include the FMC in a Monte-Carlo execution of the simulation. Instead, the offset path was automated using a localizer type directional aide (LDA) under localizer mode (LOC) for lateral flight with vertical-speed mode (VERT SPD) used to automate flight along the glidepath. The turn was automated using heading select mode (HDG SEL). Near completion of the turn, the simulation changed the ILS frequency to the runway ILS and armed both localizer and approach mode using delays as if these modes were manually armed by the crew. To stimulate flight technical errors in the aircraft, navigation errors were enabled for both the LDA and runway localizer. However, to ensure that data was collected at the same distance from the runway threshold, errors were not enabled for vertical flight. For similar reasons and to isolate the effects of navigation error as the primary cause of lateral deviation, winds, atmospheric disturbances, and errors in sensed airspeed were not enabled. The signal-in-space error for the runway localizer was set to the navigation error limits of a CAT III ILS for all runs. For the LDA, two signal-in-space errors were used. The navigation error limits of a CAT III ILS were used to examine path stability when the navigation error is the same on both the offset path and extended centerline. The navigation error limits of a CAT I ILS were used to examine path stability when the navigation error is larger on the offset path than the extended centerline. The numerical parameters for the CAT III and CAT I localizer errors were derived from data in table 13.3 of Kayton and Fried [Kayton1997].

For each combination of intercept height and localizer navigation error, 6000 runs were performed. These runs included six final approach speeds of 122 KN, 130 KT, 138 KT, 145 KT, 153 KT, and 160 KT, each of which are associated with a 10 ton increase in aircraft landing weight. These speed selections were combined with 1000 random seeds for the localizer navigation error. The simulation was configured for landings at KSFO RWY28R using the published runway and runway ILS geometry. Geometry of the LDA was derived by rotating the RWY28R ILS about the intercept point by the offset angle of 3°. Flights began at an altitude of 2600 ft and a commanded speed of 180 KT. Flights decelerated to their final approach speed starting at the FAF (1800 AGL). Characteristics of the simulation are summarized in Table 4-6.

Table 4-6 Simulation Parameters for Modified Offset Approach

Final Approach Speeds	122 KT, 130 KT, 138 KT, 145 KT, 153 KT, 160 KT
Landing weights[5]	80T, 90T, 100T, 110T, 120T, 130T
Intercept height of offset path with centerline (AGL)	370 ft, 587 ft, 730 ft, 833 ft
LDA offset	3°
CAT III Localizer Navigation Error (95%)	0.0525°
CAT I Localizer Navigation Error (95%)	0.1642°
Initial Altitude (AGL)	2600 ft
Initial Speed (EAS)	180 KT
Glidepath angle	3°
FAF height (AGL)	1800 ft
Number of runs per trial	6000

The simulation results are show in Table 4-7. To interpret the results, the maximum safe TSE at the 50 ft decision height (CAT IIIB) is ±27 ft, taken from table 13.2 of Kayton and Fried [Kayton1997]. The maximum safe TSE for the 100 ft and 200 ft DH is set at ±35 ft and ±50 ft, respectively, to accommodate expected increase in TSE with distance from threshold for an ILS approach. In all cases, TSE at the 200 ft DH improved as the intercept point moved further away from the runway threshold. TSE at 100 ft DH and 50 ft DH reach their minimums at the intercept height of 730 ft. For the CAT I LDA to CAT III ILS, which best resembles modification of the paired-approach described in the CONOPS, the aircraft cannot achieve sufficient stability on the localizer path for landing at any decision height when the intercept height is 370 ft. A couple of the behaviors observed in the simulation work against achievement of path stability this late in the approach. First, the autopilot of the simulated aircraft takes eight seconds to engage LOC mode from the time LOC is armed. Second, once the LOC mode is engaged, the aircraft appears to fly two under-damped oscillations about the path before smoothly aligning with the localizer beam. With the fastest aircraft, these behaviors require a distance of more than 0.5 NM to complete; therefore, the faster aircraft does not complete capturing of the localizer path until after the 200 ft DH for an intercept height of 370 ft. However, at the next intercept height of 587 ft, TSE does show sufficient stability across all three decision heights to conduct a landing. Moreover, the improvement is large enough that it may be possible achieve acceptable results at an intercept height between 370 and 587 ft. However, a number of secondary effects that might increase TSE or decrease its rate of decay were not enabled in the simulation. Moreover, the TSE observed on the offset path in the simulation was half as large for the CAT I LDA as the 40 m TSE assumption for the offset path in the CONOPS [MITRE2013]. Therefore, a more conservative recommendation is to compare the two scenarios of CAT III LDA to CAT III ILS and CAT I LDA to CAT III ILS, and chose the intercept height where sensitivity to TSE on the offset path disappears. This occurs beginning in the neighborhood of the 730 ft intercept height.

[5] Landing weights have a one-to-one correspondence with the approach speeds.

Table 4-7 Observed TSE at Decision Heights for Modified Offset Paired-Approach

Intercept Height (ft AGL)	Total System Error (ft, 95% bounds)					
	CAT III LDA to CAT III ILS			CAT I LDA to CAT III ILS		
	200 ft	100 ft	50 ft	200 ft	100 ft	50 ft
370	25	19	18	77	47	37
587	21	18	17	25	20	18
730	20	17	16	21	17	16
833	19	17	16	19	17	16

These results indicate that it is not possible to conduct landing at CAT II or lower minima for offset path intercept at or below 1 NM from the threshold. Therefore, the geometry for the offset paired-approach currently defined in the CONOPS cannot be extended to lower minima. The intercept point must be increased to 1.5 and 2 NM from the threshold. Extending the intercept distance, however, also constricts the wake-safe distance throughout the procedure. This constriction presents the biggest challenge on the parallel portion of the approach. For a given procedure availability, the necessary crosswind tolerance increases with altitude, reaching a near asymptote around 10 KT adverse crosswind [Audenaerd2012]. The offset portion of the approach provides relief from the increasing crosswind by increasing the distance that the wake must travel. However, the parallel portion of the approach must absorb the entire effect of increasing crosswind. The CONOPS design was validated, assuming the current fleet of aircraft in service, with a maximum near surface crosswind of 5 KT. Similar studies would need to be performed to ascertain the feasibility of extending the parallel portion of the approach with the current aircraft fleet or to determine the future performance necessary to execute this modified approach. The study, however, does suggest that, when the TSE on the offset path and turn equals that of a CAT III approach (CAT III LDA to CAT III ILS), then a late turn onto the extended centerline at 1 NM becomes possible. However, achieving similar performance on the offset path, would require next generation avionics utilizing high accuracy navigation sources like ground-based augmentation system approach service type D (GAST-D) GPS or even wide-area augmentation system (WAAS) GPS with 5 Hz update rate.

4.5. Observations

The ALAS alerting algorithm is especially effective when the aircraft are within 1 NM of the runway threshold. This is due to the significantly smaller TSE in this region. Therefore, from a collision detection viewpoint, the potential of lowering the visibility minima using a hybrid procedure is very promising. However, the high-fidelity simulation indicates that stabilizing the approach path on a CAT III ILS is possible for the current generation aircraft fleet only for intercept points at least 1.5 to 2 NM from the threshold. Assessing the aircraft capabilities necessary to conduct the offset paired-approach with the offset intercept at higher elevations will require additional simulation studies. Alternatively, the high-fidelity simulation results also suggest it may be possible to retain a 1 NM intercept distance if technology can be developed to constraint total system error to the accuracy of a straight-in CAT III ILS approach when flying the latter part of the offset path, the turn onto the extended centerline, and the extended centerline to touchdown. Such a system may be possible using GAST-D GPS or even WAAS GPS with 5 Hz update rate.

We have briefly looked at the issue of executing the escape maneuver while near to the

ground. It is conceivable that near ground blunders are extremely unlikely and perhaps they can be excluded. But if these blunders cannot be excluded, future work will be necessary to develop a more intelligent escape maneuver that differs depending on the relative position and velocity of the aircraft.

5. Conclusions

In this report we present the analytical and experimental results using the ALAS alerting algorithm in several variants of a future paired approach concept of operations. We examined the SAPA procedure for different runway spacings using a fast-time simulation and found that the SAPA procedure can be used at 950 ft separations or higher with next-generation avionics and that 1150 ft separations or higher is feasible with current-rule compliance ADS-B OUT. Both of these results depend upon the use an aggressive escape maneuver that is automatically engaged. The runway separations can be lowered an additional 50 ft if different glideslopes are used (i.e. 2.85° and 3.0). We have also conducted high-fidelity simulations at 1050 ft for next-generation avionics and 1400 ft separation for the current-rule ADS-B, which confirmed the fast-time simulations. The Joint Planning Development Office (JPDO) recently asked NASA to consider whether adding additional aircraft states, like roll angle, to ADS-B OUT could improve results; NASA has added expansion of ADS-B state data to its planned FY14 work.

We have also analyzed the use of echelon spacing for straight in approaches without the use of the ALAS alerting algorithm. The statistical analysis shows that current generation aircraft cannot conduct paired approaches on parallel paths using echelon spacing on runways less than 1400 ft apart and next-generation aircraft will not be able to conduct paired approach on runways less than 1050 ft apart. These runway separations are greater than the estimates for which passing becomes safe using the SAPA procedure (see Section 2.1.3.1). Since the SAPA approach allows passing, SAPA can more easily accommodate larger differences in approach speed and lower minimum approach speeds. However, the echelon spacing approach has a cost advantage since it requires only monitoring of lateral and longitudinal bounds while SAPA requires an alerting algorithm and an automated escape maneuver.

Finally, we looked at the use of the ALAS alerting algorithm in conjunction with the MITRE echelon concept. The goal of this work was to lower the visibility minima requirements for the MITRE CONOPS. The fast-time simulation found that the ALAS alerting algorithm was very effective when deployed starting at 1 NM from the threshold. However, for the offset paired-approach, the high-fidelity simulation showed that stabilizing the approach path on a CAT III ILS was only possible for current generation aircraft at merge points at least 1.5 to 2 NM from the threshold. Nevertheless, the high-fidelity simulation results suggest that it may be possible to retain a 1 NM intercept distance if technology can be developed to constraint total system error on the offset path and final turn. Such a system may be possible using ground-based augmentation system approach service type D (GAST-D) GPS or even wide-area augmentation system (WAAS) GPS with 5 Hz update rate. Without such technology, this hybrid approach using an offset path is not likely to be feasible at a 1 NM merge point. We have also identified an issue in using the escape maneuver near ground (e.g. 300 ft or below). Due to airport buildings and surrounding terrain, the turn component may have to be disengaged until a sufficient height is reached. Preliminary results show that this can have a serious impact on the probability of a collision. Nevertheless, the same ground obstacles can also restrict the blunder characteristics of the lead aircraft. More analysis is required to determine the limits of both blunder and escape maneuvers near the ground.

6. Future Work

In FY14, NASA plans to pursue improvements in paired-approach procedure design and the ALAS alerting algorithm to increase the availability of the paired-approach procedures while improving safety.

- Evaluate the benefits of adding roll-angle to the ADS-B OUT broadcast. Roll angle often leads the observed turn performance of the intruder aircraft. Therefore, it is possible that the broadcast of roll angle can provide earlier alerts and reduce the required runway separation for safe passing under the SAPA procedure.

- Evaluate the benefits of adding Traffic Alert and Collision Avoidance System (TCAS) slant range data as an input to the ALAS alerting algorithm. TCAS slant range has higher accuracy than slant range derived from ADS-B OUT broadcasts. It may be possible to develop alerting criteria derived from or blended with TCAS slant range data to improve alerting performance.

- Refine and enhance the performance of the ALAS alerting algorithm, based on actual aircraft position/velocity data for auto-coupled, auto-throttle approaches obtained from FAA data sources.

- Continue hybrid Paired Approach (CAT II/III) development with echelon spacing and ALAS alerting to achieve enhanced performance to lower weather minima. For echelon spacing with an offset path, assess the capabilities needed to move the merge point an additional 0.5 to 1.0 NM from the runway.

- Investigate the problem of executing an escape maneuver near the ground (e.g. 350 ft and below). Develop an intelligent escape maneuver that is based on the available positions and velocities of the aircraft.

- Integrate interval management for closely spaced parallel operations (IM-CSPO) and SAPA using flight-deck interval management (FIM) to deliver aircraft to the initiation point for SAPA and then transition to a SAPA operation.

The results in this paper and those of future work are subject to the fidelity and uncertainty of wake vortex models. Higher fidelity models of wake vortices and better characterization of model uncertainties will be necessary to increase confidence in the safety of estimated wake-free boundaries. Moreover, improved wake-vortex modeling may also reveal opportunities to accommodate closer runway spacing through adjustments in the procedure. For parallel approach procedures like SAPA, the need for improved wake-vortex characterization extends across all three regions of vortex behavior: in-ground effect (IGE), near-ground effect (NGE), and out-of-ground effect (OGE).

References

[Abbott2002] Abbott, T.S: Flight Test Evaluation of the Airborne Information for Lateral Spacing (AILS) Concept. NASA Langley Technical Paper, NASA/TM-2002-211639, 2002.

[Audenaerd2012] Audenaerd, L., A Characterization of Surface and Aloft Winds for Advanced Parallel Runway Operations, Journal of the Transportation Research Board Volume/Issue Volume 2300, Volume 2300 / 2012 Publisher Transportation Research Board of the National Academies Pages49-58 Print ISSN0361-1981 DOI10.3141/2300-06 Online Date Thursday, November 15, 2012.

[Boeing2012] The Boeing Company, "RNP Capability of FMC Equipped 737, Generation 3", Document Number D6-39067-3, Release G, June 12, 2012.

[Eckstein2011] Eckstein, Adric. "Directed FOQA Studies to Correlate Aircraft Navigation with PBN Procedure", MITRE, MITRE Technical Report 110298, July 2011.

[Eftekari2008] Eftekari, R.R., "Terminal Area RNAV/RNP Flight Path Synthesis", MITRE, unpublished, July 31, 2008.

[Eftekari2011] Eftekari, R.R.; Hammer, J.B.; Havens, D.A.; Mundra, A.D., "Feasibility analyses for paired approach procedures for closely spaced parallel runways," *Integrated Communications, Navigation and Surveilance Conference (ICNS), 2011* , pp. I5-1 to I5-14, 10-12 May 2011.

[FAA2010] FAA. "Automatic Dependent Surveillance—Broadcast (ADS–B) Out Performance Requirements To Support Air Traffic Control (ATC) Service; Final Rule." Federal Register (National Archive and Records Administration) 75, no. 103 (May 2010): 30160 - 30195.

[FAA2011] Geometrical Models For Aircraft In Terminal Area Risk Analyses, FAA Document DOT-FAA-AFS-450-63, Flight Systems Laboratory Oklahoma City, Oklahoma, April 2011.

[FAA2012] FAA. digital - Terminal Procedures Search. http://aeronav.faa.gov/digital_tpp.asp?ver=1209&eff=08-23-2012&end=09-20-2012. Washington, D.C., August 23, 2012.

[FAA-CSPO] http://www.faa.gov/about/office_org/headquarters_offices/avs/offices/afs/afs400/afs450/cspo/focus_areas/

[Garmin2012] Garmin. “Datasheet for GPS 500W, GPS 400W, and GNC 420.” https://buy.garmin.com/shop/store/assets/pdfs/specs/gps400w_spec.pdf (accessed September 4, 2012).

[Helleberg2006] Helleberg, John; Domino, David; Mundra, Anand; Mayer, Ralf. " Predicting Aircraft Approach Speeds for Enhancing Airport Capacity", AIAA 2006-6323, AIAA Guidance, Navigation, and Control Conference and Exhibit, Keystone, CO, 21 - 24 August, 2006.

[Johnson2010] Johnson, Sally C., Terrance S. Abbot, Nelson M. G. Guerreiro, Gary W. Lohr, Paul Volk, and Burnell T. McKissick. Simplified Aircraft-based Paired Approach: Concept Definition and Initial Analysis. Hampton: NASA Langley Research Center, 2010 (under review).

[Kayton1997] Kayton, Myron and Fried, Walter R. "Avionics Navigation Systems", John Wiley and Sons, Inc., New York, 1997, ISBN 0-471-54795.

[Massimini2006] Massimini, Vincent S. "Simultaneous Independent and Dependent Parallel Instrument Approaches: Assumptions, Analysis, and Rationale", MITRE, McLean, VA, 2006.

[MITRE2013] Stassen, H. Peter; Eftekari, Robert; Mundra, Anand; Domino, David A.; Haltli, Brennan; Koch, Marshall; Lekovish, Dan; Massimini, Vince; Tuomey, David, "Paired Approach Concept of Operations (CONOPS)", MITRE, MITRE Product 130081, Version 1.0, June 28, 2013.

[Mohleji2010] Mohleji, Satish C., and Ganghuai Wang. Modeling ADS-B Position and Velocity Errors for Airborne Merging and Spacing in Interval Management Application. McLean: Mitre, 2010.

[Murphy2010] Murphy, Tim. "GNSS Implementation on Commercial Air Transport Airplanes", The 14th Meeting of the APEC GNSS Implementation Team (GIT/14), Seattle, Washington, June 21-24, 2010, Presentation.

[NOAA1976] National Oceanic And Amospheric Administration, National Aeronautics And Space Administration, and United States Air Force. " U.S. Standard Atmosphere, 1976", NOAA-S/T 76-1562, U.S. Government Printing Office, Washington, D. C., 1976.

[Passerini2012] Passerini, Alex. "Qantas RNP-AR Data Review, Feb 2011 Update", Qantas Airlines, February 2011, Presentation.

[Perry2013] Perry, Raleigh B.; Michael M. Madden, Wilfredo Torres-Pomales, and Ricky W. Butler: The Simplified Aircraft-based Paired Approach with the ALAS Alerting Algorithm, NASA/TM-2013-217804.

[RTCA2002] RTCA, Inc: "Minimum Aviation System Performance Standards for Automatic Dependent Surveillance Broadcast (ADS-B)", DO-242A, Washington, D.C., June 25, 2002.

[RTCA2006] RTCA, Inc: "Minimum Operational Performance Standards for Global Positioning System / Wide Area Augmentation System Airborne Equipment", DO-229D, Washington, D.C., December 13, 2006.

[RTCA2009] RTCA, Inc: "Minimum Operational Performance Standards for 1090 MHz Extended Squitter Automatic Dependent Surveillance – Broadcast (ADS-B) and Traffic Information Services – Broadcast (TIS-B)", DO-260B, Washington, D.C., December 2, 2009.

[RTCA2011] RTCA, Inc: "Minimum Operational Performance Standards (MOPS) for Aircraft Surveillance Applications (ASA) System", DO-317A, Washington, D.C., December 13, 2011.

[Samanant2000] Samanant, Paul and Mike Jackson: “Description of the AILS Alerting Algorithm”, NASA/CR-2000-210109, May 2000.

[Shank1994] Shank, Eric M. and Katherine M. Hollister: “Precision Runway Monitor”, The Lincoln Laboratory Journal. Vol. 7. No. 2. pp. 329-353, 1994.

[Smith2000] R. Smith: “A Description of the Cockpit Motion Facility and the Research Flight Deck Simulator", AIAA-2000-4174, AIAA Modeling and Simulation Technologies Conference and Exhibit, Denver, CO, August 2000.

[Thomas1990] Thomas, James and Dominic Timoteo. "Chicago O'Hare Simultaneous ILS Approach Data Collection and Analysis", U. S. Department of Transportation, Atlantic City, NJ, Report DOT/FAA/CT-TN90/11, April 1990.

[Thomas1993] Thomas, J.; Timoteo, D.; Hoang, P. "Los Angeles International Airport Instrument Landing System Approach Data Collection and Reduction Phase 1 Final Report", U. S. Department of Transportation, Atlantic City, NJ, Report DOT/FAA/CT-TN93/12, November 1993.

[Wallis2013] Wallis S. *Binomial confidence intervals and contingency tests: mathematical fundamentals and the evaluation of alternative methods*. London: University College London; 2012. Available from: http://www.ucl.ac.uk/english-usage/staff/sean/resources/binomialpoisson.pdf.

[Warren1999] Warren, Anthony W.: “Lateral Control & Error Modeling for Precision Approach”, Boeing Commercial Airplane Group, unpublished, October 1999.

[Winder2001] Winder, L. W. and James K. Kuchar: "Generalized Philosophy of Alerting with Application to Parallel Approach Collision Prevention", AIAA Guidance, Navigation, and Control Conference, Montreal, Canada, August 6-9, 2001.

Appendix A. New Offset Runway Conformance Algorithm

The previous version of the ALAS Alerting algorithm was designed for fully parallel approaches only. However, the latest version of the algorithm and software enables runway conformance testing on merged approaches. The algorithm is illustrated in the Figure A-1:

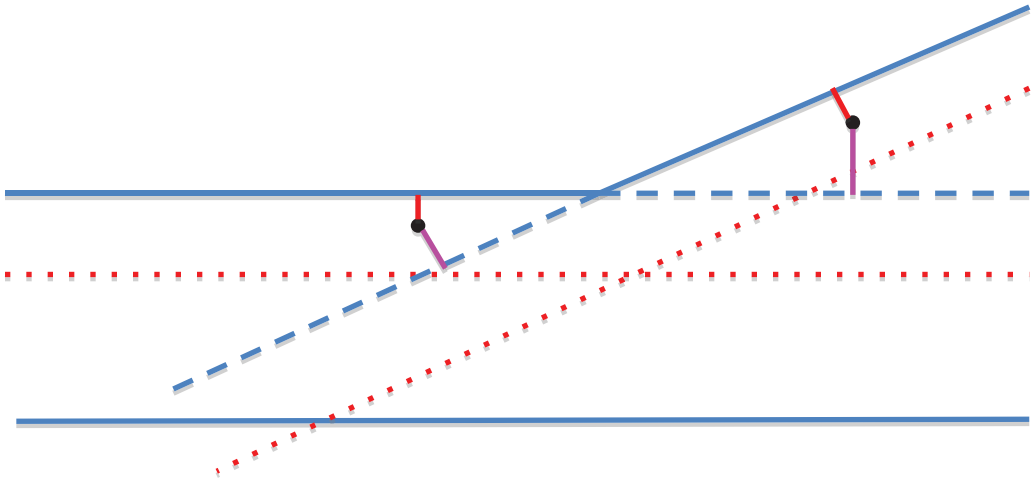

Figure A-1: Offset runway conformance bounds

The runway centerlines are solid lines. The dotted red lines show the maximum deviation before an alert is issued. The runway centerlines are extended with dashed lines. The algorithm measures the perpendicular distance from both runway centerlines. The safe side distance is given a negative sign and hence becomes a negative number. The maximum distance is used as the runway deviation. This maximum distance is compared to two positive parameters values: yellowRunwayDist and redRunwayDist. If the distance exceeds these values an alert is issued.

If the position vectors are Euclidean the calculation is straight-forward:

$$t = (q - s) \bullet v \,/\, v \bullet v$$

$$\text{Distance} = \| s + t\, v - q \|$$

If the position vectors are given in geodesic coordinates:

Compute the "cross track distance" as defined by the Aviation Formulary (v1.44) by Ed Williams. This function forms a great circle from two points on the centerline (p1, p2). It then computes the shortest distance of another point (off Circle) to the great circle:

```
cross_track_distance(p1, p2, offCircle) {
dist_p1oc = angular_distance(p1,offCircle);
trk_p1oc = initial_course_impl(p1,offCircle,dist_p1oc);
trk_p1p2 = initial_course(p1,p2);
//This is a direct application of the "spherical law of sines"
return distance_from_angle(asin(sin(dist_p1oc)*sin(trk_p1oc-trk_p1p2)),
        (p1.alt()+p2.alt()+offCircle.alt())/3.0);
```

Thus far we have not performed any simulations using this new ALAS capability. The algorithm has been coded in both Java and C++ and is ready for experimental use in future work.

Appendix B. tAlas Simulation Validation

B.1. Results for Cylinder Protection Zone and No Escape Maneuver

In this section we present the results of a baseline run, executing the tAlas simulation with no alerting and no escape maneuver. This is important to insure that the simulation is generating blunders that will lead to collisions if not detected.

Table B-1: Results for Various Runway Spacings with No Escape Maneuver

Runway Spacing (ft)	Num Los	Probability	Minimum Distance (ft)
750	1,863,967	1.86E-01 ± 1.23E-04	0.86
850	1,682,885	1.68E-01 ± 1.18E-04	0.48
950	1,521,025	1.52E-01 ± 1.14E-04	0.87
1050	1,375,997	1.38E-01 ± 1.09E-04	0.26
1150	1,245,431	1.25E-01 ± 1.04E-04	1.13
1250	1,129,458	1.13E-01 ± 1.00E-04	0.41
1350	1,025,597	1.03E-01 ± 9.59E-05	0.25
1450	932,246	9.32E-02 ± 9.19E-05	0.86

Comparing this table with Table 2-5 shows us that the ALAS alerting algorithm provides at least 4 orders of magnitude improvement.

B.2. Impact of maxT2 on Blunder Angle of Incidence

The T2 parameter controls the duration of the blunder turn. This value will determine the maximum angle of incidence of the intrusion onto the ownship's centerline.

Table B-2: Angle of Incidence of Blunders For Runway 1050 ft, 1.5 s latency as a function of MaxT2

MaxT2	Maximum Incidence Angle (°)	Average Incidence Angle (°)
10	30.94	7.90
11	33.58	8.54
12	36.17	9.17
13	41.50	9.86
14	46.97	10.63
15	52.47	11.47
16	56.60	12.37

Table B-3: Angle of Incidence of Blunders For Runway 750 ft, 1.5 s latency as a function of MaxT2

MaxT2	Maximum Incidence Angle (°)	Average Incidence Angle (°)
10	30.78	8.11
11	33.40	8.73
12	35.99	9.35
13	41.32	10.02
14	46.14	10.78
15	50.12	11.59
16	51.63	12.42

For a given runway spacing there is a maximum angle of incidence onto the ownship's centerline that can be achieved. For a 1050 ft runway the maximum angle of incidence is a bit over 30 degrees. Increasing maxT2 increases the frequency of more aggressive maneuvers and hence increases the probability of a LoS.

B.3. Track Rate Threshold Sensitivity

The performance of the Alas alerting algorithm is strongly dependent upon the trackRateThreshold parameter. The collision detection component of the algorithm is engaged when the intruder's averaged turn rate exceeds the value of this parameter. If it is set too low, there will be too many false alarms. If it is set too high, then the alert will be delayed longer. In Table B-4 the impact of this parameter is shown for the 950 ft runway spacing case and in Table B-5 the impact on the 1050 ft runway spacing case is shown. Note that acceptable probabilities are indicated in blue font and unacceptable probabilities are indicated in red.

Table B-4: Simulation Runs for 950 ft Runway using Different Track Rate Thresholds

Track Rate Threshold (°/s)	Probability (400 ft)	Probability (large cylinder)	Minimum Distance (ft)
1.0	1.40E-04 ± 3.74E-06	3.34E-06 ± 5.58E-07	258.65
1.1	2.11E-04 ± 4.59E-06	7.84E-06 ± 8.73E-07	218.96
1.2	3.13E-04 ± 5.59E-06	1.58E-05 ± 1.25E-06	212.68
1.5	8.50E-04 ± 9.21E-06	7.69E-05 ± 2.77E-06	157.66
2.0	2.96E-03 ± 1.72E-05	4.37E-04 ± 6.61E-06	58.79

Using the large cylinder protection zone, values of this parameter of 1.2 or larger resulted in collision probabilities that are beyond our target value of 1E-05/landing. There were some CMF runs where false alarms were seen, but the latest version of ALAS used for generating the fast-time results in this paper does not exhibit false alarms for these runs. The trackRateThreshold parameter was set at 1.0 °/s for these runs.

Table B-5: Simulation Runs for 1050 ft Runway using Different Track Rate Thresholds

Track Rate Threshold (°/s)	Probability (400 ft)	Probability (large cylinder)	Minimum Distance (ft)
1.0	9.84E-06 ± 9.81E-07	4.38E-07 ± 1.48E-07	316.55
1.1	1.77E-05 ± 1.32E-06	5.38E-07 ± 1.79E-07	292.52
1.2	3.18E-05 ± 1.78E-06	7.38E-07 ± 2.28E-07	292.15
1.5	1.34E-04 ± 3.67E-06	6.24E-06 ± 7.76E-07	240.72
2.0	7.11E-04 ± 8.43E-06	7.96E-05 ± 2.82E-06	141.78

Note that if the trackRateThreshold parameter were increased to 1.5 °/s, then the 950 runway spacing would no longer be available, but the 1050 runway spacing would still be practical. We do not expect that the parameter will need to be this large because in the CMF simulation results we very rarely see any track rates above 0.5 °/s. We hope to test the behavior of the ALAS algorithm on real landing data to tune this parameter to its optimal value. Also, there is potential to improve the averaging filter that is used in the algorithm if real landing data becomes available.

Appendix C. Measuring ALAS False Alarm Rate Using MITRE/Boeing TSE Model

Our fast-time simulation tAlas was used to measure the false alarm rate of ALAS. For this experiment, the ownship's protection zone was defined as a moving quadrant D distance away from the ownship's centerline in the direction of the intruder and X units behind the ownship, as illustrated in Figure C-1. The protection zone extends forward from the ownship all the way to the runway to account for the possibility of a catastrophic wake encounter if the intruder were to cross in front of the ownship. Crossing behind the ownship is considered safe (for the ownship). The area to the side of the ownship away from the intruder is included in the protection zone as this is where the ownship would escape in case of a red alert. A blunder was defined as any intruder trajectory that entered the ownship's protection zone. A false alarm occurs when ALAS issues a red alert on an intruder trajectory that does not carry it into the ownship's protection zone.

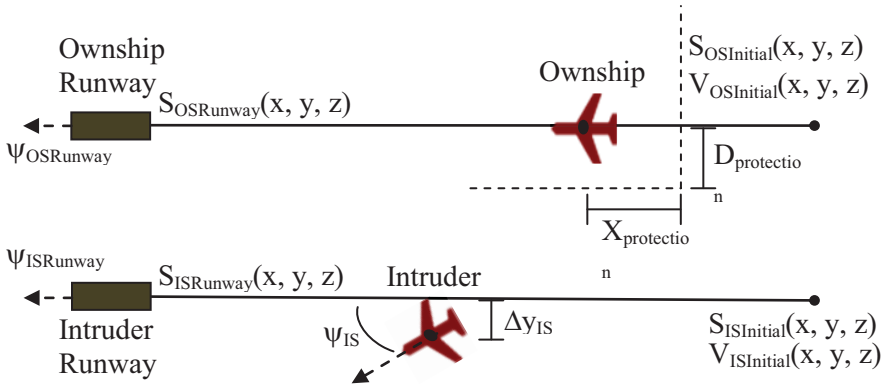

Figure C-1: Top view of the scenario for measuring the false alarm rate

To measure the false alarm rate, we ran landing trials in which the aircraft followed their respective glide paths at constant ground speeds. These trials used a random lateral error model tuned for a typical distribution of deviations from the centerline for both the ownship and the intruder. This model is described in the next section. There were no blundering trajectories during these tests. The aircraft were given initial positions on their glide paths between 7 and 8 NM from the runways with a longitudinal separation between 1000 and 1500 ft. The ground speeds ranged between 114 and 160 KT with a maximum speed difference of 15 KT. The protection zone parameters were set to X = 400 ft and D = 230 ft. The landing trials ran for 400 seconds of simulated time or until the altitude of one or both aircraft dropped below 100 ft above ground level. We ran four sets of landings, each with 7,290,000 landing trials. Only the TrackRate Threshold of ALAS changed between the sets of landings. All other parameters of ALAS and the test trajectories remained constant. Two statistics were collected for each set of trials: the number of red alerts issued by ALAS and the number of false alarms. As there were no blunders in any of these landing trials, the false alarm rate was equal to the number of red alerts divided by the number of trials.

C.1. Lateral Error Model

The simulation of the lateral motion of the aircraft used a flight technical error (FTE) model from MITRE [Eftekari2008], which was based on a lateral control model for final precision

approach developed by Boeing [Warren1999]. This parameterized model can be tuned to the characteristics of any aircraft and simulates effects of path disturbances due to closed loop guidance errors, wind and gusts. The model consists of a pair of differential equations for the aircraft lateral deviation Δy and track angle ψ relative to the centerline.

$$d\Delta y/dt = \mathrm{v} * \psi$$

$$d\psi/dt = -k_1 * \psi - k_2 * \Delta y + \varepsilon$$

The variables Δy and ψ are illustrated in Figure C-1 for the intruder aircraft. Δy is in units of feet per second and ψ has units of radians. Variable v denotes the aircraft airspeed in units of feet per second. Parameters k_1 and k_2 are control gains. The input ε is a noise error process representing centerline deviations of the track angle.

This model describes a second order closed-loop system with disturbance ε. The control gains are related to the damping constant ξ and natural frequency ω as follows.

$$k_1 = 2\xi\omega$$

$$k_2 = \omega^2/\mathrm{v}$$

The natural frequency ω in units of radians is related to the frequency f in Hz and the period p in seconds.

$$\omega = 2\pi\mathrm{f} = 2\pi/\mathrm{p}$$

For the simulations to measure the false alarm rate of ALAS, the damping constant ξ had a range from 0.3 to 0.5 and the period p had a range from 55 to 65 seconds.

The input ε represents disturbances acting on the aircraft and causing deviations of the track angle, which then cause lateral deviations from the centerline. The error model is parameterized with the standard deviation of the lateral error σ_y. This is derived from the FTE bound defined as the 95% containment lateral error.

σ_y = FTE/1.96

The FTE can be inferred from the least accurate RNP level for aircraft under consideration for the simulation. These aircraft are assumed to be equipped with GPS flight management systems.

FTE = (minimum RNP)/1.38

So:

σ_y = (minimum RNP)/2.705

The disturbance ε is modeled with a Johnson distribution given as a reshaped Normal distribution with slight higher probabilities at the extreme ends of the value range.

$\varepsilon = z_j * \sigma_\varepsilon$

$z_j = e^{(z/2.18)} - e^{(-z/2.18)}$

$z = x/\sigma_\varepsilon$

$x = N(0, \sigma_\varepsilon)$, a Gaussian random process with 0 mean and σ_ε standard deviation

$\sigma_\varepsilon = (2*k_1*k_2*\sigma_y^2/v)^{1/2}$

For the false alarms runs the FTE was set to 60 ft.

C.2. Results and Analysis

Table C-2 shows the measured false alarm rates as a function of the TrackRate Threshold. As would be expected, the false alarm rate decreases as the alarm threshold is relaxed. The false alarm rate was significant for a threshold of 1.0, which is the current value set through a tuning process for the ALAS parameters.

Table C-2: False alarm rate results

ALAS TrackRate Threshold	False Alarm Rate
0.7	47.36%
1.0	24.72%
1.5	2.20%
2.0	0.14%

It is known that the performance of ALAS is sensitive to the value of the TrackRate Threshold parameter as this is used to trigger the sweep algorithm that predicts blunder trajectories. Any intruder trajectory with a track rate exceeding the set threshold and a predicted potential intrusion into the front or back buffer of the ownship triggers a red alert. ALAS has a low pass filter intended to reduce the sensitivity to track rate noise, but the attenuation must be balanced with the amount of signal lag (i.e., timing delay) introduced by the filter. This lag delays the triggering of red alerts and impacts the performance of the ownship's escape maneuver.

A quick examination of the lateral error model reveals that the track rate is a direct function of the noisy disturbance ε. Thus, although the model may be representative of actual patterns of lateral error deviation, it is our judgment that the track rate is not representative. We know that the trajectories generated by the CMF high-fidelity simulations do not contain as much track rate noise. Based on this, we decided not to use this lateral error model to measure the performance of ALAS or tune its parameters. We will continue to use in tAlas the simple sinusoidal oscillation model for the lateral error until a more representative stochastic model is available.

REPORT DOCUMENTATION PAGE

Form Approved
OMB No. 0704-0188

1. REPORT DATE *(DD-MM-YYYY)*	2. REPORT TYPE	3. DATES COVERED *(From - To)*
01-01-2014	Technical Memorandum	

4. TITLE AND SUBTITLE

Analysis and Simulation of the Simplified Aircraft-Based Paired Approach Concept With the ALAS Alerting Algorithm in Conjunction With Echelon and Offset Strategies

5a. CONTRACT NUMBER

5b. GRANT NUMBER

5c. PROGRAM ELEMENT NUMBER

6. AUTHOR(S)

Torres-Pomales, Wilfredo; Madden, Michael M.; Butler, Ricky W.; Perry, Raleigh B.

5d. PROJECT NUMBER

5e. TASK NUMBER

5f. WORK UNIT NUMBER

031102.02.07.05.9D78.13

7. PERFORMING ORGANIZATION NAME(S) AND ADDRESS(ES)

NASA Langley Research Center
Hampton, VA 23681-2199

8. PERFORMING ORGANIZATION REPORT NUMBER

L-20346

9. SPONSORING/MONITORING AGENCY NAME(S) AND ADDRESS(ES)

National Aeronautics and Space Administration
Washington, DC 20546-0001

10. SPONSOR/MONITOR'S ACRONYM(S)

NASA

11. SPONSOR/MONITOR'S REPORT NUMBER(S)

NASA/TM-2014-218151

12. DISTRIBUTION/AVAILABILITY STATEMENT

Unclassified - Unlimited
Subject Category 03
Availability: NASA CASI (443) 757-5802

13. SUPPLEMENTARY NOTES

14. ABSTRACT

This report presents analytical and simulation results of an investigation into proposed operational concepts for closely spaced parallel runways, including the Simplified Aircraft-based Paired Approach (SAPA) with alerting and an escape maneuver, MITRE's echelon spacing and no escape maneuver, and a hybrid concept aimed at lowering the visibility minima. We found that the SAPA procedure can be used at 950 ft separations or higher with next-generation avionics and that 1150 ft separations or higher is feasible with current-rule compliant ADS-B OUT. An additional 50 ft reduction in runway separation for the SAPA procedure is possible if different glideslopes are used. For the echelon concept we determined that current generation aircraft cannot conduct paired approaches on parallel paths using echelon spacing on runways less than 1400 ft apart and next-generation aircraft will not be able to conduct paired approach on runways less than 1050 ft apart. The hybrid concept added alerting and an escape maneuver starting 1 NM from the threshold when flying the echelon concept. This combination was found to be effective, but the probability of a collision can be seriously impacted if the turn component of the escape maneuver has to be disengaged near the ground (e.g. 300 ft or below) due to airport buildings and surrounding terrain. We also found that stabilizing the approach path in the straight-in segment was only possible if the merge point was at least 1.5 to 2 NM from the threshold unless the total system error can be sufficiently constrained on the offset path and final turn.

15. SUBJECT TERMS

Aircraft Spacing; Airports; Flight Paths; Kinematics; Simulators; System Warnings

16. SECURITY CLASSIFICATION OF:			17. LIMITATION OF ABSTRACT	18. NUMBER OF PAGES	19a. NAME OF RESPONSIBLE PERSON
a. REPORT	b. ABSTRACT	c. THIS PAGE			STI Help Desk (email: help@sti.nasa.gov)
					19b. TELEPHONE NUMBER *(Include area code)*
U	U	U	UU	77	(443) 757-5802